IN-64

154177

P.73

Accurate Computation and Continuation of Homoclinic and Heteroclinic Orbits for Singular Perturbation Problems

M. J. Friedman and A. C. Monteiro

NASA

NASA Contractor Report 4503

Accurate Computation and Continuation of Homoclinic and Heteroclinic Orbits for Singular Perturbation Problems
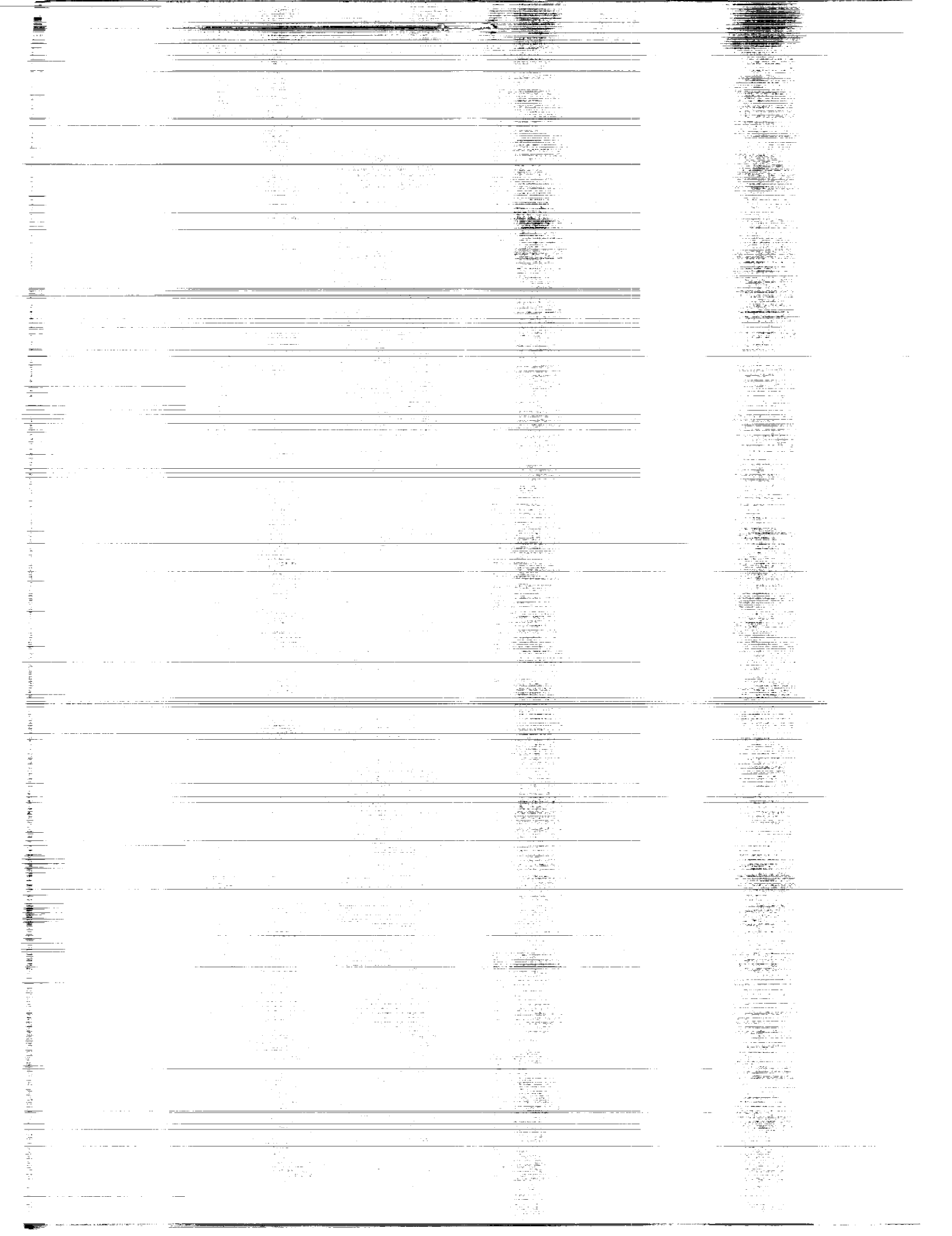
M. J. Friedman and A. C. Monteiro
The University of Alabama in Huntsville
Huntsville, Alabama

NASA

National Aeronautics and
Space Administration

Office of Management

Scientific and Technical
Information Program

1993

ACKNOWLEDGMENT

TABLE OF CONTENTS

LIST OF ILLUSTRATIONS

0. Introduction.

This project has been motivated by the study of turbulent fluid boundary layers in the wall region (Aubry et al. [1]). Numerical investigations of models for the dynamics of fluctuations in the boundary layer reveal th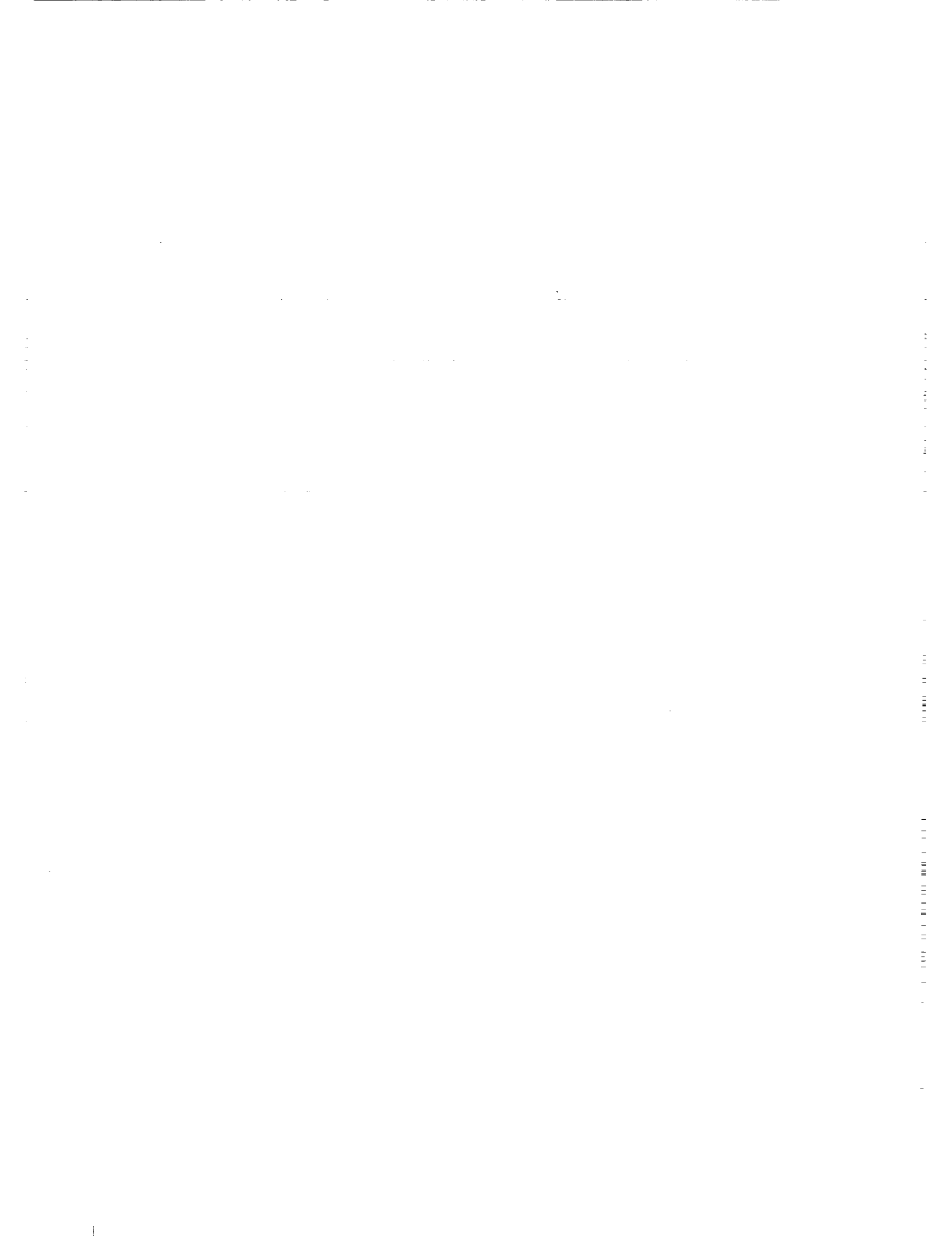e presence of intermittent solutions ("bursts") that are persistent over a range of parameter values in the model and that correspond to heteroclinic cycles in the model equations. Armbruster et al. [2] concluded, using the dynamical systems analysis, that these intermittent solutions of the model are an essential feature and not accidental.

In earlier papers [7, 8, 10, 11, 16] Doedel and Friedman have developed an accurate, robust, and systematic method for computing branches of *homoclinic and heteroclinic* orbits. These are orbits of an infinite period connecting two fixed points of an associated system of autonomous ordinary differential equations. Homoclinic orbits have been shown to play a fundamental role in phenomena such as bursting in biology, chaotic vibrations of structures, chaotic oscillations in chemical reactions, etc. Heteroclinic orbits are equally important in the understanding of the global behavior of dynamical systems and also in the study of wave phenomena in nonlinear parabolic partial differential equations.

The original goal of this project was to accurately compute heteroclinic cycles and to investigate numerically how these cycles evolve as the problem parameters vary in a model 4-dimensional system studied in [1] and [2]. This model system is a singular perturbation problem. Since homoclinic and heteroclinic orbits often arise in the context of singular perturbation problems, this project has evolved into the development of general efficient algorithms for such situations. We developed our algorithms using model 2- and 3- dimensional problems studied by Deng [12].

The organization of the paper is as follows. We first formulate the problem and describe some algorithms for computation of branches of homoclinics and heteroclinics. Then we describe application of these algorithms to several problems of interest.

1. Formulation of the Problem and Review of Some Earlier Results.

In earlier papers [7, 8, 10] Doedel and Friedman have considered the problem of finding a branch of solutions of the system of autonomous ordinary differential equations

(1.1)
$$a) \quad u'(t) - f(u(t), \lambda) = 0, \quad u(\cdot), \; f(\cdot, \cdot) \in \mathbf{R}^n, \; \lambda \in \mathbf{R}^{n_\lambda},$$
$$b) \quad \lim_{t \to -\infty} u(t) = u_0, \quad \lim_{t \to \infty} u(t) = u_1.$$

The method utilizes the linear approximation of the unstable (for $t < T_-$, $-T_- > 0$, large) and stable (for $t > T_+$, $T_+ > 0$, large) manifolds, under the assumption that solutions of (1.1) decay exponentially to their limits at $\pm\infty$. Since every translation of a solution of Eq. (1.1) is also a solution, to remove this "phase" indeterminacy we need to add a constraint. The equation

(1.2)
$$\int_{-\infty}^{\infty} \big(f(u(t), \lambda) - f(q(t), \lambda^0) \big) \cdot \frac{\partial}{\partial t} f(u(t), \lambda) dt = 0$$

seems to be, computationally, the most appropriate way to do this. It is obtained by requiring that the current solution $u(t)$ be as "close" as possible to the previously computed solution $q(t)$ (see [7] for the discussion). Our principle result, Theorem 2 in [10] can be summarized as follows:

Let (q, λ^0) be a solution of (1.1), (1.2). Assume that $n_\lambda = 2 - (n_u^- + n_s^+ - n) \geq 0$, where n_u^- and n_s^+ are dimensions of the unstable and stable manifolds of u_0 and u_1 respectively. Under appropriate assumptions on f and appropriate transversality conditions, in a neighborhood of (q, λ^0) there exists an unique solution branch $(u(s), \lambda(s))$, $(u(0), \lambda(0)) = (q, \lambda^0)$, of (1.1), (1.2) and for sufficiently large $-T_-$, T_+ an unique branch $(u(s), \lambda_T(s))$ of approximate solutions. Here s is the continuation (such as pseudo-arclength, employed by AUTO) parameter.

Moreover, we have an error estimate

(1.3)
$$\| \lambda(s) - \lambda_T(s) \|_{\mathbf{R}^{n_\lambda}} + \| u(s) - u_T(s) \|_{W^1_\infty(\mathbf{R})} \leq C \Big(e^{2T_- \mu_0} + e^{2T_+ \mu_1} \Big),$$

for some $\mu_0 > 0 > \mu_1$.

Similar results were obtained in Beyn [3, 4].

In Friedman and Doedel [11] and Friedman [16] the numerical method and its analysis have been extended to the case of center manifolds and higher order approximation of the unstable and stable manifolds.

Continuation algorithm 1. ([10]). The algorithm is based on the following equations:

(1.4)
$$u'(t) - Tf(u(t), \lambda) = 0, \quad 0 < t < 1,$$

(1.5)
$$a) \quad f(u_0, \lambda) = 0,$$
$$b) \quad f(u_1, \lambda) = 0,$$

2

$$
\text{(1.6)} \quad
\begin{array}{ll}
a) & f_u(u_0, \lambda) w_{0i} = \mu_{0i} w_{0i}, \quad w_{0i} \in \mathbf{R}^n, \ \mu_{0i} \in \mathbf{R}, \ i = 1, ..., n_0, \\[2mm]
b) & f_u(u_1, \lambda) w_{1i} = \mu_{1i} w_{1i}, \quad w_{1i} \in \mathbf{R}^n, \ \mu_{1i} \in \mathbf{R}, \ i = 1, ..., n_1,
\end{array}
$$

$$
\text{(1.7)} \quad
\begin{array}{ll}
a) & |w_{0i}| = 1, \ i = 1, ..., n_0, \\[2mm]
b) & |w_{1i}| = 1, \ i = 1, ..., n_1,
\end{array}
$$

$$
\text{(1.8)} \quad \int_0^1 \left(f(u(t), \lambda) - f(q(t), \lambda^0) \right) \cdot f_u(u(t), \lambda) f(u(t), \lambda) \, dt = 0,
$$

$$
\text{(1.9)} \quad
\begin{array}{ll}
a) & u(0) = u_0 + \epsilon_0 \sum_{i=1}^{n_0} c_{0i} w_{0i}, \quad \sum_{i=1}^{n_0} c_{0i}^2 = 1, \\[4mm]
b) & u(1) = u_1 + \epsilon_1 \sum_{i=1}^{n_1} c_{1i} w_{1i}, \quad \sum_{i=1}^{n_1} c_{1i}^2 = 1.
\end{array}
$$

Here for $x, y \in \mathbf{R}^n$ $x \cdot y$ denotes the inner product in $\mathbf{R}^n$, and we denote by $|\cdot|$ the l^2 norm in $\mathbf{R}^n$; we shall keep the same notation for the inner product and the norm for finite dimensional Euclidian spaces of dimension other then n. The above equations constitute a system of ordinary differential equations subject to constraints. In concrete cases the number of constraints (and correspondingly, the number of scalar variables) can often be significantly reduced by simple algebra and variations on the normalization equations. Equation (1.4) is the differential equation. It is obtained by truncating (1.1a) to an interval $[T_-, T_+]$, $T_- < 0 < T_+$, setting $T = |T_-| + T_+$ and then scaling the independent variable t so that it varies from 0 to 1. The actual period T therefore appears explicitly in (1.4), whereas T_- and T_+ do not appear explicitly in (1.4) – (1.9). There are n_λ problem parameters, viz., λ_i, $i = 1, ..., n_\lambda$. Equation (1.5) defines two fixed points of the vector field. In (1.6a) we assume that the Jacobian $f_u(u_0, \lambda)$ has n_0 distinct real positive eigenvalues μ_{0i} with eigenvectors w_{0i}, and $n - n_0$ real nonpositive eigenvalues. Similarly, in (1.6b) we assume that the Jacobian $f_u(u_1, \lambda)$ has n_1 distinct real negative eigenvalues μ_{1i} with eigenvectors w_{1i}, and $n - n_1$ real nonnegative eigenvalues. Under appropriate assumptions on f, by the stable manifold theorem the fixed point u_0 has a (strongly) unstable manifold of dimension n_0 to which the linear subspace $S_0 \equiv \text{Span}(\{w_{0i}\}_{i=1}^{n_0})$ is tangent at u_0. The fixed point u_1 has a (strongly) stable manifold of dimension n_1 to which the linear subspace $U_1 \equiv \text{Span}(\{w_{1i}\}_{i=1}^{n_1})$ is tangent at u_1.

We have $w_{0i}, w_{1i}, u_0, u_1 \in \mathbf{R}^n$. Equation (1.9a) then requires that the starting point $u(0)$ of the orbit $u(t)$ lie in the tangent manifold S_0 at "distance" ϵ_0 from the fixed point u_0. Similarly, equation (1.9b) requires the endpoint $u(1)$ to lie in U_1 at "distance" ϵ_1 from the fixed point u_1. Finally (1.8) represents the *"phase condition"*.

The unknowns u_0 and u_1 can be eliminated entirely from (1.4)–(1.9) by using (1.9). Then (1.4)–(1.8) represent n coupled differential equations subject to $n_c =$

$2n + (n + 1)(n_0 + n_1) + 3$ constraints, of which (1.9) is an integral condition. In addition to the vector function variable $u(t) \in \mathbf{R}^n$ we have scalar variables

$$\lambda \in \mathbf{R}^{n_\lambda}, \quad \epsilon_0, \epsilon_1 \in \mathbf{R},$$

(1.10)
$$\mu_{0i}, c_{0i} \in \mathbf{R}, \quad w_{0i} \in \mathbf{R}^n, \quad i = 1, ..., n_0,$$

$$\mu_{1i}, c_{1i} \in \mathbf{R}, \quad w_{1i} \in \mathbf{R}^n, \quad i = 1, ..., n_1.$$

The total number of scalar variables equals $n_v \equiv n_\lambda + (n + 2)(n_0 + n_1) + 2$. Formally we need $n_v = n_c - n$ for a single heteroclinic connection. Usually we are interested in computing an entire *branch* (one dimensional continuum) of orbits, in which case $n_v = n_c - n + 1$. This requirement is equivalent to setting the number of free problem parameters

(1.11)
$$n_\lambda = n - (n_0 + n_1) + 2.$$

The period T is kept fixed in the continuation. For T large and ϵ_0 and ϵ_1 small, each solution on the branch represents an approximate heteroclinic connection. If we want to increase the period T, then we can replace one of the problem parameters, say λ_1, by T (see [10] for an example of such a computation).

2. New Algorithms for Computation of Homoclinic and Heteroclinic Orbits.

We formulate the algorithms in the situation when the unstable (stable) manifold is 1-dimensional, while the stable (unstable) manifold can have dimension greater than 1. See also Monteiro [13]. In this case the direction along the unstable (stable) manifold is locally defined by the eigenvector corresponding to the positive (negative) eigenvalue, while it is more difficult to determine what linear combination of eigenvectors defines locally the direction along the stable (unstable) manifold. To be specific and without loss of generality, we assume that the eigenvector w_0^u defines the direction of the one-dimensional unstable manifold $W_{loc}^u(u_0)$ at the fixed point u_0.

Starting orbits can be obtained by using either AUTO itself or some initial value solver. In applications we used KAOS [14] and VODE [15].

Continuation algorithm 2 (floating boundary algorithm). Eqs. (1.4) – (1.9) are modified by dropping the equations which define the direction along the stable manifold. The equations now are:

$$(2.1) \qquad u'(t) - Tf(u(t), \lambda) = 0, \quad 0 < t < 1,$$

$$(2.2) \qquad f(u_0, \lambda) = 0,$$

$$(2.3) \qquad f_u(u_0, \lambda)w_0^u = \mu_0^u w_0^u, \quad w_0^u \in \mathbf{R}^n, \ \mu_0^u \in \mathbf{R},$$

$$(2.4) \qquad |w_0^u| = 1,$$

$$(2.5) \qquad \int_0^1 \left(f(u(t), \lambda) - f(q(t), \lambda^0) \right) \cdot f_u(u(t), \lambda)f(u(t), \lambda)\, dt = 0,$$

$$(2.6) \qquad u(0) = u_0 + \epsilon_0 w_0^u,$$

The unknown u_0 can be eliminated from (2.1)-(2.5) by using (2.6). Then (2.1)-(2.5) represent n coupled differential equations subject to $n_c = 2n + 2$ constraints. In addition to the vector function variable $u(t) \in \mathbf{R}^n$ we have scalar variables

$$(2.7) \qquad \begin{array}{l} \lambda \in \mathbf{R}^{n_\lambda}, \ \epsilon_0 \in \mathbf{R}, \\ \mu_0^u \in \mathbf{R}, \ w_0^u \in \mathbf{R}^n. \end{array}$$

The total number of scalar variables equals $n_v \equiv n_\lambda + n + 2$. As in [7] we are interested in computing an entire *branch* (one dimensional continuum) of orbits, in which case the number of free problem parameters

$$(2.8) \qquad n_\lambda = 1.$$

Continuation algorithm 3 (steering vector algorithm). The equations for this algorithm are:

$$(2.9) \qquad u'(t) - Tf(u(t), \lambda) = 0, \quad 0 < t < 1,$$

$$(2.10) \qquad \begin{aligned} f(u_0, \lambda) &= 0, \\ f(u_1, \lambda) &= 0, \end{aligned}$$

$$(2.11) \qquad f_u(u_0, \lambda) w_0^u = \mu_0^u w_0^u, \quad w_0^u \in \mathbf{R}^n, \ \mu_0^u \in \mathbf{R},$$

$$(2.12) \qquad \begin{aligned} |d| &= 1, \\ |w_0^u| &= 1, \end{aligned}$$

$$(2.13) \qquad \int_0^1 \left(f(u(t), \lambda) - f(q(t), \lambda^0) \right) \cdot f_u(u(t), \lambda) f(u(t), \lambda) \, dt = 0,$$

$$(2.14) \qquad \begin{aligned} a) \quad & u(0) = u_0 + \epsilon_0 w_0^u, \\ b) \quad & u(1) = u_1 + \epsilon_1 d, \qquad d \in \mathbf{R}^n. \end{aligned}$$

Again the unknowns u_0 and u_1 can be eliminated from (2.9)–(2.13), by using (2.14). Then (2.9)–(2.13), represent n coupled differential equations subject to $n_c = 3n + 3$ constraints. In addition to the vector function variable $u(t) \in \mathbf{R}^n$ we have $n_v \equiv n_\lambda + 2n + 3$ scalar variables

$$(2.15) \qquad \lambda \in \mathbf{R}^{n_\lambda}, w_0^u, d \in \mathbf{R}^n, \quad \epsilon_0, \epsilon_1, \mu_0^u \in \mathbf{R}.$$

Again we are interested in computing an entire *branch* (one dimensional continuum) of orbits, in which case we have

$$(2.16) \qquad n_\lambda = 1, \text{ and hence } n_v = 2n + 4.$$

6

We next give two algorithms for obtaining starting orbits, which can be used in conjunction with Continuation algorithms 1–3.

Starting orbit algorithm 1 (IVP Solver)

Step 1 *Assume that u_0, w_0^u, and λ are given with $|w_0^u| = 1$. Initialize the "distance" ϵ_0 by "small" number, such as 0.0001 and compute the initial value*

$$(2.17) \qquad\qquad u(0) = u_0 + \epsilon_0 w_0^u.$$

This provides an initial value for an initial value solver such as KAOS [14]. Next solve the initial value problem: (2.17), (2.18),

$$(2.18) \qquad\qquad u'(t) - Tf(u(t), \lambda) = 0, \quad 0 < t < 1,$$

for "large" time T, such as 20 – 100.

Step 2 *Switch to AUTO. Initialize u_0, w_0^u, μ, T and λ from step 1. Read the data generated by KAOS and interpolate it. This provides an initial orbit $u(t)$ for AUTO.*

Step 3. *Perform continuation by one of the Continuation algorithms 1–3. Note that in the case of the Continuation algorithm 1, one first needs to compute the projection of $u(1)$ found at Step 1 onto the subspace spanned by w_{1i}, $i = 1, ..., n_1$.*

Starting orbit algorithm 2 (floating boundary).

Step 1. *Initialize the period T by a "small" number, such as 0.01, and the "distance" ϵ_0 by another "small" number, such as 0.0001. Given u_0 and w_0^u, initialize the solution by a constant:*

$$(2.19) \qquad\qquad u(t) = u_0 + \epsilon_0 w_0^u, \ 0 < t < 1.$$

Step 2 *Perform continuation in the direction of increasing T, while all other parameters are fixed, using the equations*

$$(2.20) \qquad\qquad u'(t) - Tf(u(t), \lambda) = 0, \quad 0 < t < 1,$$

$$(2.21) \qquad\qquad u(0) = u_0 + \epsilon_0 w_0^u.$$

Starting orbit algorithm 3 (steering vector).

Step 1. *Initialize the period T by a "small" number, such as 0.01, and the "distance" ϵ_0 by another "small" number, such as 0.0001. Given u_0 and w_0^u, initialize the solution by a constant:*

$$(2.22) \qquad\qquad u(t) = u_0 + \epsilon_0 w_0^u, \ 0 < t < 1.$$

and initialize d, ϵ_1 from the equations:

$$(2.23) \qquad\qquad \begin{aligned} u_1 + \epsilon_1 d &= u_0 + \epsilon_0 w_0^u, \\ |d| &= 1. \end{aligned}$$

<u>Step 2</u> *Perform continuation in the direction of increasing T using the equations*

(2.24)
$$u'(t) - Tf(u(t), \lambda) = 0, \quad 0 < t < 1,$$

(2.25)
$$a) \quad u(0) = u_0 + \epsilon_0 w_0^u,$$
$$b) \quad u(1) = u_1 + \epsilon_1 d, \qquad d \in \mathbf{R}^n$$

(2.26)
$$|d| = 1,$$
$$|w_0^u| = 1.$$

Remark. The integral "phase" condition is removed for the *Floating Boundary* and the *Steering Vector* algorithms because its purpose is to prevent the sharp peaks from moving. In this method the peaks must move to approach the heteroclinic orbit from the constant solution. AUTO allows the user to set the accuracy to which the variables and parameters are computed in the continuation procedure, by varying the tolerances. In the beginning of the continuation one must set high tolerances for the parameters and variables, because the constant solution is per se a poor approximation of a heteroclinic orbit.

3. A Model 2–d Singular Perturbation Problem.

3.1 Formulation of the Problem.

The system of equations given below is a model problem which we have used to develop our algorithms in the case of Singular Perturbation Problems,

$$
\begin{aligned}
\dot{x} &= (2 - z)a(x - 2) + (z + 2)[\alpha(x - x_0) + \beta(y - y_0)] \\
\text{(3.1)} \quad \dot{y} &= (2 - z)[d(b - a)(x - 2)/4 + by] + (z + 2)[-\beta(x - x_0) + \alpha(y - y_0)] \\
\epsilon\dot{z} &= (4 - z^2)[z + 2 - m(x + 2)] - \epsilon c z
\end{aligned}
$$

From Deng [12], it is known that for the parameter values $a = 1, b = 1.5, c = 2, m = 1.1845, \alpha = 0.01, \beta = 5, x_0 = -0.1, y_0 = -2, \epsilon = 0.01, d = -3.5$ the solution is a twisted homoclinic orbit, while with the same values of parameters except $d = -0.2$ the orbit is nontwisted.

Singular perturbation problems are characterized by the appearance of a small parameter such as $\epsilon = 0.01$, which in this case makes the system of ordinary differential equations a stiff system. Stiff equations are systems where the magnitude of one eigenvalue of the Jacobian is considerably greater than the magnitude of the other eigenvalues.

In this system of equations, it is known that a hyperbolic fixed point exists at $w_0 = (2, 0, -2)$. The eigenvalues of the Jacobian evaluated at (2,0,-2) are $(\mu_1, \mu_2, \mu_3) \approx (-1847, 5, 3)$ with associated eigenvectors (w_1^s, w_1^u, w_2^u). The eigenvalue $\mu_1 = -1847$ is responsible for the stiffness of the system. The eigenvector w_1^s gives the local direction of the stable manifold, while some linear combination of (w_1^u, w_2^u) defines the direction of the unstable manifold.

Computing the homoclinic orbit for the 3–dimensional problem is formidable for 3 reasons: (1) the system of equations in Eq. (3.1) is stiff. (2) It is known theoretically that the direction of the unstable manifold $W_{loc}^u(u_0)$ is defined only by the eigenvector w_1^s. However for the numerically approximate problem (which we solve) both w_1^u and w_2^u will define the direction of $W_{loc}^u(u_0)$ and the linear combination of w_1^u and w_2^u is unknown. (3) There are several heteroclinic orbits near the homoclinic orbit, and the slightest numerical instability will displace the homoclinic orbit to one of these heteroclinic orbits. In view of these reasons, we decided to compute a 2-dimensional homoclinic orbit, to gain some insight into the intricacies of computing the full 3–dimensional orbit. There was also the *possibility* that we could then compute the 3–d orbit by a *homotopy* from the 2–d orbit.

For the 2–d problem the stable and unstable manifolds, $W_{loc}^s(u_0)$ and $W_{loc}^u(u_0)$ are each one–dimensional.

We attempt to compute homoclinic orbits for the two dimensional system of equations, obtained from Eq. (3.1) by setting $\dot{y} = 0$ and $y = 3.59 \times 10^{-3}$ (since it is known that for the 3–d system $(x, y, z) = (1.99, 3.59 \times 10^{-3}, -1.99)$ is a fixed point):

$$
\begin{aligned}
\text{(3.2)} \quad \dot{x} &= (2 - z)a(x - 2) + (z + 2)[\alpha(x - x_0) + \beta(y - y_0)] \\
\dot{z} &= ((4 - z^2)[z + 2 - m(x + 2)] - \epsilon c z)/\epsilon
\end{aligned}
$$

9

3.2 Computational Results

We use the following notation:

$u_0 = (u_{01}, u_{02})$ Fixed Point

$w_1^u = (w_{11}^u, w_{12}^u)$ Eigenvector tangent to the unstable manifold at u_0

$w_1^s = (w_{11}^s, w_{12}^s)$ Eigenvector tangent to the stable manifold at u_0

$d_1 = (d_{11}, d_{12})$ Normalized steering vector components connecting $u(1)$ and u_0

ϵ_0 Distance between u_0 and $u(0)$

ϵ_1 Distance between u_0 and $u(1)$

$u_0, w_1^u, w_2^u, d_1, u(0), u(1) \in \mathbf{R}^2$

$\epsilon_0, \epsilon_1 \in \mathbf{R}$

$\lambda = (\epsilon, d) \in \mathbf{R}^2$

To compute a homoclinic orbit for this system of equations we use the steering vector algorithm and after noting that for a homoclinic orbit The homoclinic orbit is obtained for Eq. (3.1) by a series of steps.

Step 1 (a): Obtain an initial homoclinic orbit for

(3.3)
$$u' = Tf(u, \lambda), \quad u = (x, z)$$

subject to the boundary conditions:

(3.4)
$$(a) \ u(0) = u_0 + \epsilon_0 w_1^u$$
$$(b) \ u(1) = u_0 + \epsilon_1 d_1$$

and normalization condition,

(3.5)
$$|d_1| = 1$$

for a total of 5 boundary conditions. Note that $d_1 = (d_{11}, d_{12}) \in \mathbf{R}^2$. Initialize $T = 0.01$, $\epsilon_0 = 10^{-7}$, $u_0 = (1.99, -1.99)$, $w_1^u = (1.0, -5.2 \times 10^{-4})$ and the tolerances $\epsilon_u, \epsilon_\lambda = 10^{-2}$. Begin computation of the orbit along the unstable manifold. Perform continuation with respect to $T, d_{11}, d_{12}, \epsilon_1$ using the steering vector algorithm for obtaining initial orbits. We have now reached Fig. (3.1), where $(d = -0.2, \epsilon = 0.01, \epsilon_0 = 1.0 \times 10^{-6}, T = 1.15 \times 10^{-2}, \mu_1^s = -1891)$, $(\mu_1^u = 3.99, w_{11}^u = 0.99, w_{12}^u = -5.0 \times 10^{-4})$, $(\epsilon_1 = 1.0 \times 10^{-6}, d_{11} = -0.99, d_{12} = 5.2 \times 10^{-4})$, $(u_{01} = 1.99, u_{02} = -1.99)$.

Step 1 (b): Decrease the tolerances so that $\epsilon_u, \epsilon_\lambda = 10^{-8}$. Perform continuation with respect to $T, d_{11}, d_{12}, \epsilon_1$ until d_1 has approximately the same direction as the eigenvector w_1^s, which defines the direction of the stable manifold $W_{loc}^s(u_0)$ near the fixed point. The computation reaches Fig. (3.2) where $\epsilon_1 = 0.078$. In Fig. (3.2) $(d = -0.2, \epsilon = 0.01, \epsilon_0 = 1.0 \times 10^{-6}, T = 3.89, \mu_1^s = -1891)$, $(\mu_1^u = 3.99, w_{11}^u = 0.99, w_{12}^u = -5.0 \times 10^{-4})$, $(\epsilon_1 = 0.078, d_{11} = -0.42, d_{12} = 0.90)$, $(u_{01} = 1.99, u_{02} = -1.99)$.

Step 2 (a): Switch from the steering vector algorithm to the eigenvector algorithm on the right boundary (stable manifold). The problem is formulated as follows:

$$u' = Tf(u, \lambda), \quad u = (x, z)$$

(3.6)

with the boundary conditions

(3.7)
$$(a)\ u(0) = u_0 + \epsilon_0 w_1^u$$
$$(b)\ u(1) = u_0 + \epsilon_1 d_1$$

eigenvalue problem conditions

(3.8)
$$(a)\ f_u^0 w_1^u = \mu_1^u w_1^u$$
$$(b)\ f_u^0 d_1 = \mu_1^s d_1$$

normalization conditions

(3.9)
$$(a)\ |w_1^u| = 1$$
$$(b)\ |d_1| = 1$$

and the fixed point conditions

(3.10)
$$f(u_0, \lambda) = 0$$

We now have a total of 12 boundary conditions. At this point in the computation, the direction of the steering vector is only an approximation to the eigenvector which defines the direction of the stable manifold on the right boundary. Therefore, the tolerances for the state variables and the parameters should be set rather high when switching from the steering vector approximation to the eigenvector approximation. Experimentally we found that we needed $\epsilon_u, \epsilon_\lambda = 1$. Perform a few steps of continuation ($NMX = 5$) with respect to $T, \epsilon, \epsilon_1, d_{11}, d_{12}, w_{11}^u, w_{12}^u, \mu_1^u, \mu_1^s, u_{01}, u_{02}$ for a total of 11 parameters. Note the presence of the singular perturbation parameter ϵ. After this step of continuation, the components d_{11}, d_{12} will be aligned along the direction of the eigenvector, which defines the direction of the stable manifold. We have now reached Fig. (3.3) where $\epsilon_1 = 0.0752$ and $d_1 = (d_{11} = -5.91 \times 10^{-3}, d_{12} = 0.99998)$, is now aligned along the eigenvector w_1^s, but

the singular perturbation parameter has changed its value to $\epsilon = 0.0111645$. In Fig. (3.3) the parameter values are $(d = -0.2, \epsilon = 0.0116, \epsilon_0 = 1.0 \times 10^{-6}, T = 3.85, \mu_1^s = -1693)$, $(\mu_1^u = 3.99, w_{11}^u = 0.99, w_{12}^u = -5.89 \times 10^{-4})$, $(\epsilon_1 = 0.07, d_{11} = -5.9 \times 10^{-3}, d_{12} = 0.99)$, $(u_{01} = 1.99, u_{02} = -1.99)$.

Step 2 (b): Decrease the tolerances to $\epsilon_u, \epsilon_\lambda = 10^{-8}$ and proceed with continuation as in Step 2(a). The singular perturbation parameter ϵ increased in value from 0.01 to about 1.11, whence the orbit obtained was homoclinic. At intermediate values of ϵ_1 the orbit is not homoclinic. For example for $\epsilon_1 = 0.371$, the orbit is not homoclinic. The orbit obtained for $\epsilon_1 = 1.117774$ is shown in Fig. (3.4), where it is clear that the orbit is homoclinic. The parameter values in Fig. (3.4) are $(d = -0.2, \epsilon = 1.12, \epsilon_0 = 1.0 \times 10^{-6}, T = 8.75, \mu_1^s = -11)$, $(\mu_1^u = 2.85, w_{11}^u = 0.99, w_{12}^u = -0.079)$, $(\epsilon_1 = 5.3 \times 10^{-13}, d_{11} = -0.59, d_{12} = 0.80)$, $(u_{01} = 1.20, u_{02} = -1.71)$.

Step 3: Attempt to decrease ϵ back to the value of 0.01. Freeze the period T from Step 2(b) and perform continuation with respect to $\epsilon, \epsilon_0, \epsilon_1, d_{11}, d_{12}, w_{11}^u, w_{12}^u, \mu_1^u, \mu_1^s, u_{01}, u_{02}$ using the same set of boundary conditions described in Step 2(a). A surprising result was noted: (1) ϵ returned to a value of 0.011117. (2) ϵ_0 had started at a value $\epsilon_0 = 10^{-6}$ in Step 1, but on this return journey, it reached a value of $\epsilon_0 = -2.0 \times 10^{-12}$ and $\epsilon_1 = 1.117 \times 10^{-9}$. This final orbit is shown in Fig. (3.5). The parameter values in Fig. (3.5) are $(d = -0.2, \epsilon = 0.011, \epsilon_0 = -2.7 \times 10^{-10}, T = 8.75, \mu_1^s = -1693)$, $(\mu_1^u = 3.99, w_{11}^u = 0.99, w_{12}^u = -5.9 \times 10^{-4})$, $(\epsilon_1 = 1.1 \times 10^{-9}, d_{11} = -5.9 \times 10^{-3}, d_{12} = 0.99)$, $(u_{01} = 1.99, u_{02} = -1.99)$.

Step 4: We now attempt to compute a branch of homoclinic orbits with respect to (d, ϵ). Add the integral phase condition and formulate the problem as follows:

$$u' = Tf(u, \lambda), \quad u = (x, z)$$

(3.11)

with the boundary conditions

(3.12)
$$(a)\ u(0) = u_0 + \epsilon_0 w_1^u$$
$$(b)\ u(1) = u_0 + \epsilon_1 d_1$$

eigenvalue problem conditions

(3.13)
$$(a)\ f_u^0 w_1^u = \mu_1^u w_1^u$$
$$(b)\ f_u^0 d_1 = \mu_1^s d_1$$

normalization conditions

(3.14)
$$(a)\ |w_1^u| = 1$$
$$(b)\ |d_1| = 1$$

12

and the fixed point conditions

$$(3.15) \qquad\qquad\qquad f(u_0, \lambda) = 0$$

$$(3.16) \qquad\qquad \int_{-\infty}^{\infty} \left(f(u(t), \lambda) - f(q(t), \lambda^0) \right) \cdot \frac{d}{dt} f(u(t), \lambda) dt = 0$$

Now perform continuation with respect to $\epsilon, d, \epsilon_0, \epsilon_1, d_{11}, d_{12}, w_{11}^u, w_{12}^u, \mu_1^u, \mu_1^s, u_{01}, u_{02}$. This is now a two parameter continuation problem with respect to the parameters (ϵ, d). The parameter d starts at $d = -0.2$ and continues on until $d = -8000$ without any significant change in the orbit. The stiffness of the problem is not altered by this variation in the parameter d.

3.3 Figures

Fig. 3.1. $(d = -0.2, \epsilon = 0.01, \epsilon_0 = 1.0 \times 10^{-6}, T = 1.15 \times 10^{-2}, \mu_1^s = -1891)$, $(\mu_1^u = 3.99, w_{11}^u = 0.99, w_{12}^u = -5.0 \times 10^{-4})$, $(\epsilon_1 = 1.0 \times 10^{-6}, d_{11} = -0.99, d_{12} = 5.2 \times 10^{-4})$, $(u_{01} = 1.99, u_{02} = -1.99)$.

Fig. 3.2. $(d = -0.2, \epsilon = 0.01, \epsilon_0 = 1.0 \times 10^{-6}, T = 3.89, \mu_1^s = -1891)$, $(\mu_1^u = 3.99, w_{11}^u = 0.99, w_{12}^u = -5.0 \times 10^{-4})$, $(\epsilon_1 = 0.078, d_{11} = -0.42, d_{12} = 0.90)$, $(u_{01} = 1.99, u_{02} = -1.99)$.

Fig. 3.3. $(d = -0.2, \epsilon = 0.0116, \epsilon_0 = 1.0 \times 10^{-6}, T = 3.85, \mu_1^s = -1693)$, $(\mu_1^u = 3.99, w_{11}^u = 0.99, w_{12}^u = -5.89 \times 10^{-4})$, $(\epsilon_1 = 0.07, d_{11} = -5.9 \times 10^{-3}, d_{12} = 0.99)$, $(u_{01} = 1.99, u_{02} = -1.99)$.

Fig. 3.4. $(d = -0.2, \epsilon = 1.12, \epsilon_0 = 1.0 \times 10^{-6}, T = 8.75, \mu_1^s = -11)$, $(\mu_1^u = 2.85, w_{11}^u = 0.99, w_{12}^u = -0.079)$, $(\epsilon_1 = 5.3 \times 10^{-13}, d_{11} = -0.59, d_{12} = 0.80)$, $(u_{01} = 1.20, u_{02} = -1.71)$.

Fig. 3.5. $(d = -0.2, \epsilon = 0.011, \epsilon_0 = -2.7 \times 10^{-10}, T = 8.75, \mu_1^s = -1693)$, $(\mu_1^u = 3.99, w_{11}^u = 0.99, w_{12}^u = -5.9 \times 10^{-4})$, $(\epsilon_1 = 1.1 \times 10^{-9}, d_{11} = -5.9 \times 10^{-3}, d_{12} = 0.99)$, $(u_{01} = 1.99, u_{02} = -1.99)$.
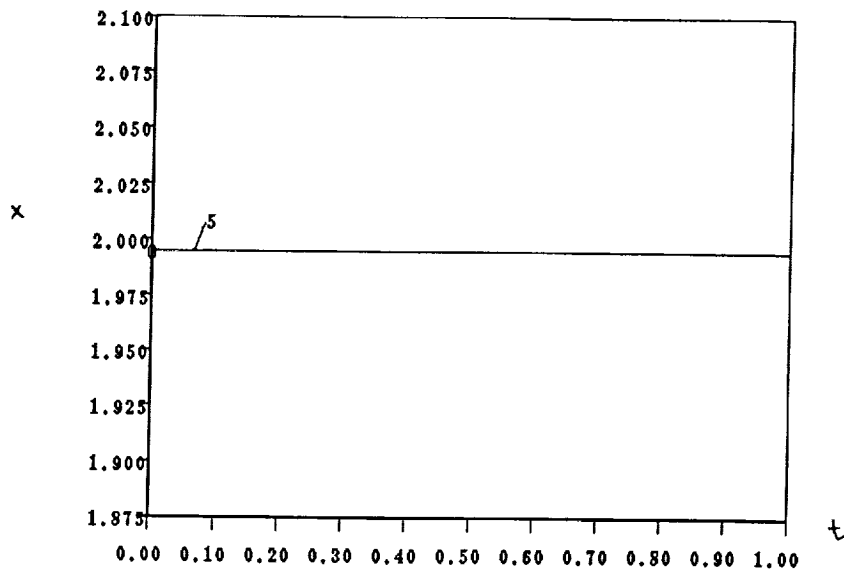
FIGURE 3.1
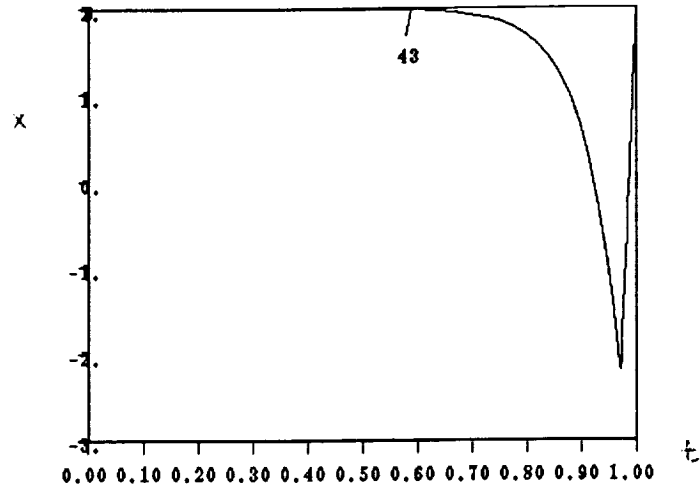
```
  d
  DIMENSION :    3
  ENTER AXES  (DEFAULT   2  3),  <D> (DISPLAY), OR <EX> (EXIT)
lab
     INVALID COMMAND,  REENTER
  DIMENSION :    3
  ENTER AXES  (DEFAULT   2  3),  <D> (DISPLAY), OR <EX> (EXIT)
2d

  THE LABELS ARE :       1    2    3    4    5    6    7    8    9   10
                        11   12   13   14   15   16   17   18   19   20
                        21   22   23   24   25   26   27   28   29   30
                        31   32   33   34   35   36   37   38   39   40
                        41   42   43   44   45   46   47   48   49   50
```

FIGURE 3.2
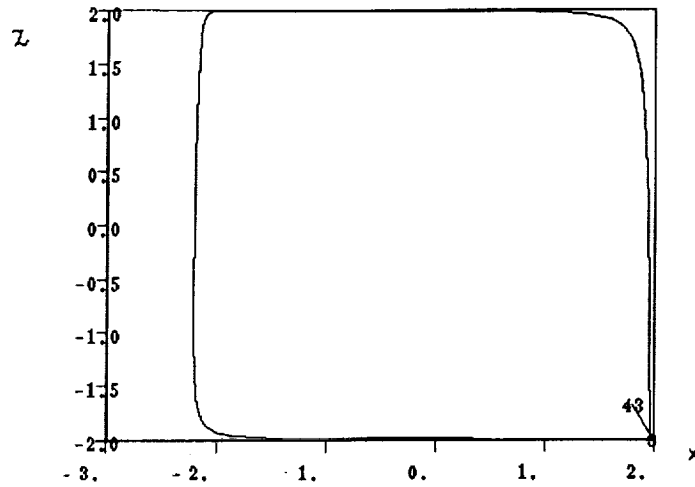
```
                          31  32  33  34  35  36  37  38  39  40
                          41  42  43  44  45  46  47  48  49  50
                          52  53  54  55  56  57  58  59  60  62
                          63  64  65  66  67  68  69  70  71  72
                          73  74  75  76  77  78  79  80  81  82
                          83  84  85  86  87  88  89  90  91  92
                          93  94  95
 ENTER NEW LABELS :
43
   DIMENSION :    3
   ENTER AXES  (DEFAULT   1  2),  <D> (DISPLAY), OR <EX> (EXIT)
d
   DIMENSION :    3
   ENTER AXES  (DEFAULT   1  2)   <D> (DISPLAY)  OR <EX> (EXIT)
```

FIGURE 3.2 (Con't.)

16

```
      ENTER AXES  (DEFAULT   1  3),  <D> (DISPLAY), OR <EX> (EXIT)
   2 3
      DIMENSION :    3
      ENTER AXES  (DEFAULT   2  3),  <D> (DISPLAY), OR <EX> (EXIT)
   d
      DIMENSION :    3
      ENTER AXES  (DEFAULT   2  3),  <D> (DISPLAY), OR <EX> (EXIT)
   2d

      THE LABELS ARE :      1    2    3    4    5    6    7    8    9   18
                           11   12   13   14   15   16   17   18   19   28
                           21   22   23   24   25   26   27   28   29   38
                           31   32   33   34   35   36   37   38   39   48
                           41   42   43   44   45   46   47   48   49   58
```

FIGURE 3.3

```
  ENTER AXES  (DEFAULT  2  3),  <D> (DISPLAY), OR <EX> (EXIT)
2d

  THE LABELS ARE :      1    2    3    4    5    6    7    8    9   18
                       11   12   13   14   15   16   17   18   19   28
                       21   22   23   24   25   26   27   28   29   38
                       31   32   33   34   35   36   37   38   39   48
                       41   42   43   44   45   46   47   48   49   58
                       52   53   54   55   56   57   58   59   68   62
                       63   64   65   66   67   68   69   78   71   72
                       73   74   75   76   77   78   79   88   81   82
                       83   84   85   86   87   88   89   98   91   92
                       93   94   95

  ENTER NEW LABELS :
```

FIGURE 3.3 (Con't.)
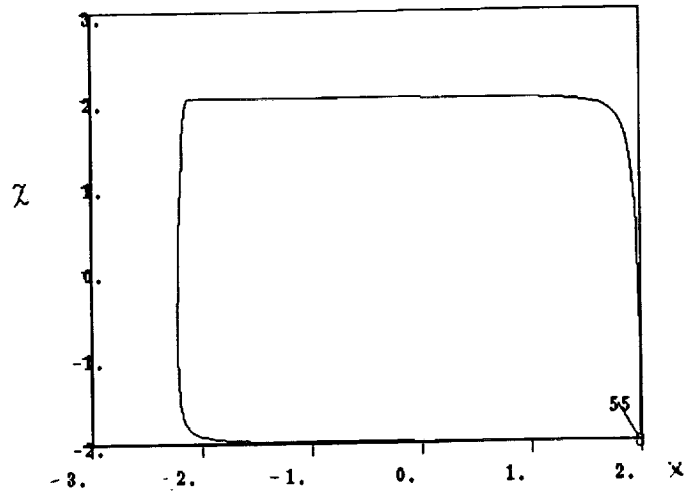
```
                    31  32  33  34  35  36  37  38  39  40
                    41  42  43  44  45  46  47  48  49  50
                    52  53  54  55  56  57  58  59  60  62
                    63  64  65  66  67  68  69  70  71  72
                    73  74  75  76  77  78  79  80  81  82
                    83  84  85  86  87  88  89  90  91  92
                    93  94  95
 ENTER NEW LABELS :
55
   DIMENSION :    3
   ENTER AXES  (DEFAULT  1  2),  <D> (DISPLAY), OR <EX> (EXIT)
d
   DIMENSION :    3
   ENTER AXES  (DEFAULT  1  2),  <D> (DISPLAY), OR <EX> (EXIT)
```
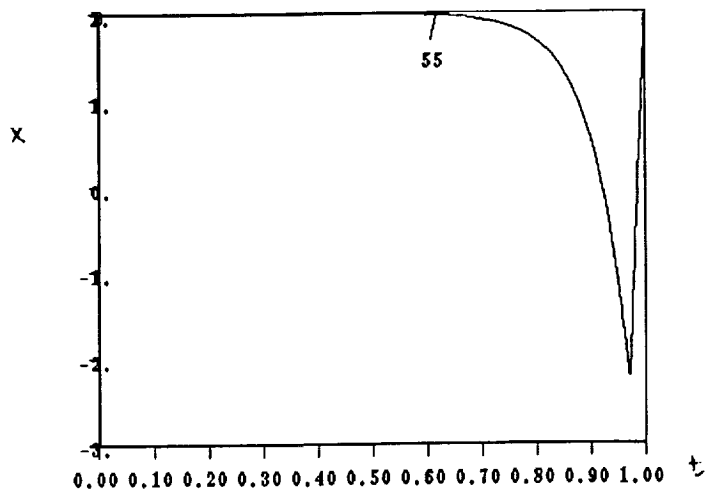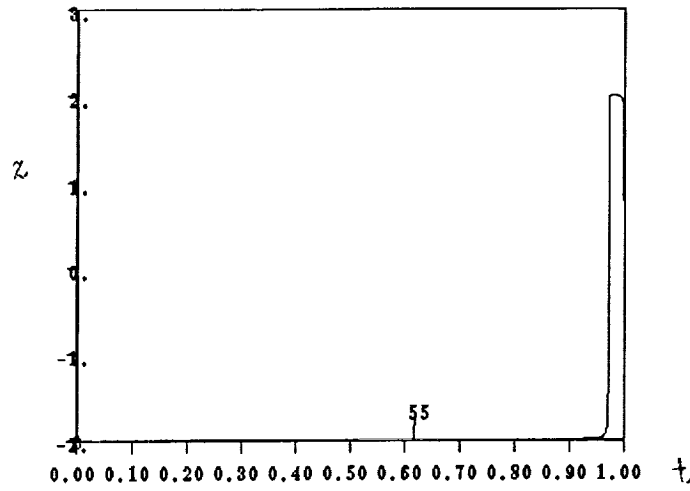
FIGURE 3.3 (Con't.)

19

```
     ENTER AXES  (DEFAULT   1  3),  <D> (DISPLAY), OR <EX> (EXIT)
   2 3
     DIMENSION :     3
     ENTER AXES  (DEFAULT   2  3),  <D> (DISPLAY), OR <EX> (EXIT)
   d
     DIMENSION :     3
     ENTER AXES  (DEFAULT   2  3),  <D> (DISPLAY), OR <EX> (EXIT)
   2d

     THE LABELS ARE :      1     2     3     4     5     6     7     8     9    10
                          11    12    13    14    15    16    17    18    19    20
                          21    22    23    24    25    26    27    28    29    30
                          31    32    33    34    35    36    37    38    39    40
```

FIGURE 3.4

```
    -0.70
    -0.80
    -0.90
    -1.00
 χ  -1.10
    -1.20
    -1.30
    -1.40
    -1.50
    -1.60
    -1.70
    -1.80
        0.00 0.10 0.20 0.30 0.40 0.50 0.60 0.70 0.80 0.90 1.00   t
```

```
  ENTER AXES  (DEFAULT   2  3),  <D> (DISPLAY), OR <EX> (EXIT)
 2d

    THE LABELS ARE :      1    2    3    4    5    6    7    8    9   18
                         11   12   13   14   15   16   17   18   19   28
                         21   22   23   24   25   26   27   28   29   38
                         31   32   33   34   35   36   37   38   39   48
                         41   42   43   44   45   46   47   48   49   58
                         52   53   54   55   56   57   58   59   68   62
                         63   64   65   66   67   68   69   78   71   72
                         73   74   75   76   77   78   79   88   81   82
                         83   84   85   86   87   88   89   98   91   92
                         93   94   95
   ENTER NEW LABELS :
```
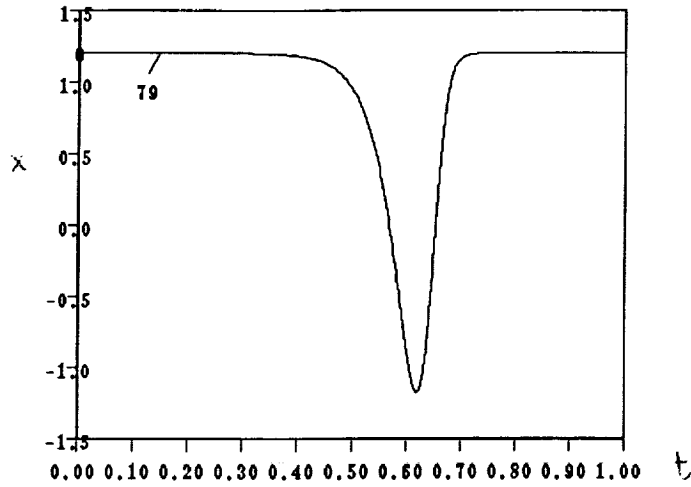
FIGURE 3.4 (Con't.)

21

FIGURE 3.4 (Con't.)

FIGURE 3.4 (Con't.)

The graph shows a plot with z (vertical axis) from -2.0 to 2.0 and t (horizontal axis) from 0.00 to 1.00. A label "94" appears near t=0.55.

Screen text below the graph:

```
ENTER AXES  (DEFAULT   2  3),  <D> (DISPLAY), OR <EX> (EXIT)
2d

THE LABELS ARE :      1    2    3    4    5    6    7    8    9   10
                     11   12   13   14   15   16   17   18   19   20
                     21   22   23   24   25   26   27   28   29   30
                     31   32   33   34   35   36   37   38   39   40
                     41   42   43   44   45   46   47   48   49   50
                     52   53   54   55   56   57   58   59   60   62
                     63   64   65   66   67   68   69   70   71   72
                     73   74   75   76   77   78   79   80   81   82
                     83   84   85   86   87   88   89   90   91   92
                     93   94   95

ENTER NEW LABELS :
```

FIGURE 3.4 (Con't.)

24

FIGURE 3.5

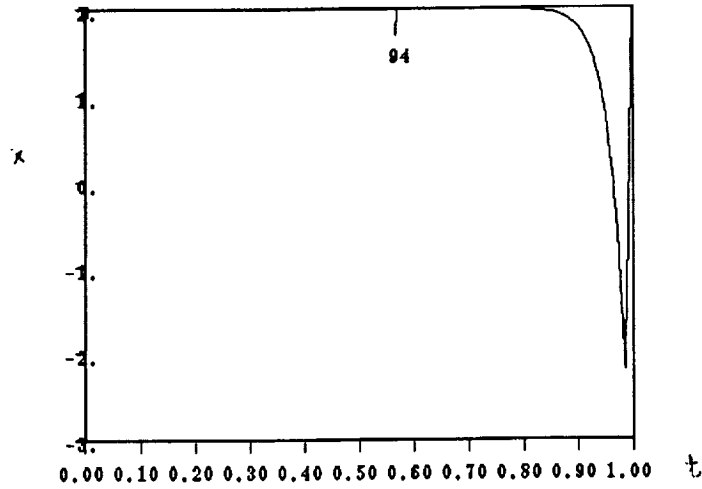# 4. A Model 3–d Singular Perturbation Problem

4.1 Formulation of the Problem

The system of equations given below is the model problem for applying continuation algorithms to Singular Perturbation Problems,

$$\dot{x} = (2 - z)a(x - 2) + (z + 2)[\alpha(x - x_0) + \beta(y - y_0)]$$
$$(4.1) \qquad \dot{y} = (2 - z)[d(b - a)(x - 2)/4 + by] + (z + 2)[-\beta(x - x_0) + \alpha(y - y_0)]$$
$$\epsilon\dot{z} = (4 - z^2)[z + 2 - m(x + 2)] - \epsilon c z$$

From Deng [12], it is known that for the parameter values $a = 1, b = 1.5, c = 2, m = 1.1845, \alpha = 0.01, \beta = 5, x_0 = -0.1, y_0 = -2, \epsilon = 0.01, d = -3.5$ the solution is a twisted homoclinic orbit, while with the same values of parameters except $d = -0.2$ the orbit is nontwisted.

Singular perturbation problems are characterized by the appearance of a small parameter such as $\epsilon = 0.01$, which in this case makes the system of ordinary differential equations stiff. Stiff equations are systems where the magnitude of one eigenvalue of the Jacobian is considerably greater than the magnitude of the other eigenvalues.

In this system of equations, it is known [12] that there exists a hyperbolic fixed point near $u_0 = (2, 0, -2)$ for $(\epsilon, d) = (0.01, -0.2)$. A more accurate solution with the IMSL subroutine DNEQNF yields $u_0 = (1.99469, 3.59524 \times 10^{-3}, -1.997886)$ for Eq. (4.1). The eigenvalues of the Jacobian evaluated at u_0 are $(\mu_1^s, \mu_1^u, \mu_2^u) \approx (-1891, 3.99, 5.99)$ with associated eigenvectors $w_1^s = (-5.3 \times 10^{-3}, 5.5 \times 10^{-3}, 0.99)$, $w_1^u = (0.99, 5.2 \times 10^{-2}, -5.2 \times 10^{-4})$, $w_2^u = (5.2 \times 10^{-3}, 0.99, -2.7 \times 10^{-6})$. The eigenvalue $\mu_1^s = -1891$ is responsible for the stiffness of the system. The eigenvector w_1^s gives the local direction of the stable manifold $W_{loc}^s(u_0)$, while some linear combination of (w_1^u, w_2^u) defines the direction of the unstable manifold $W_{loc}^u(u_0)$.

To compute the non-twisted homoclinic orbit, we used the **steering vector algorithm**. The boundary $u(0)$ was displaced from the fixed point u_0 by ϵ_0 along the eigenvector w_1^u as outlined in [13]; this corresponded to the unstable manifold. The boundary $u(1)$ was attached to the steering vector d_1. The results of the computation are shown in the attached Figures.

4.2 Computational Results.

Drawing on insight obtained from the two dimensional problem, we attempted to compute homoclinic orbits for the three dimensional system :

$$(4.2) \qquad u' = Tf(u, \lambda), \quad u = (x, y, z)$$

which symbolically represent Eq. (4.1). To compute a homoclinic orbit for this system of equations, we will go through a number of steps, with each step having a different set of boundary conditions.

We use the following notation:

$u_0 = (u_{01}, u_{02}, u_{03})$ Fixed Point

$w_1^u = (w_{11}^u, w_{12}^u, w_{13}^u)$ First eigenvector tangent to the unstable manifold at u_0

$w_2^u = (w_{21}^u, w_{22}^u, w_{23}^u)$ Second eigenvector tangent to the unstable manifold at u_0

$w_1^s = (w_{11}^s, w_{12}^s, w_{13}^s)$ Eigenvector tangent to the stable manifold at u_0

$d_1 = (d_{11}, d_{12}, d_{13})$ Normalized steering vector components connecting $u(1)$ and u_0

ϵ_0 Distance between u_0 and $u(0)$

ϵ_1 Distance between u_0 and $u(1)$

Step 1 (a): Initialize $T = 0.01$, $\epsilon_0 = 10^{-7}$, $(\epsilon, d) = (0.01, -0.2)$ and set the tolerances to $\epsilon_u, \epsilon_\lambda = 10^{-2}$. We attempt to start computing the homoclinic orbit along the unstable manifold $W_{loc}^u(u_0)$ from the boundary $u(0)$. $W_{loc}^u(u_0)$ is defined by some linear combination of the eigenvectors, (w_1^u, w_2^u). This linear combination is not known *a priori*, so following Deng [12] we start the computation of the orbit along the eigenvector w_1^u. We obtain an initial orbit for Eq. (4.1) formulated as follows:

$$(4.3) \qquad u' = Tf(u, \lambda), \quad u = (x, y, z)$$

with the 6 boundary conditions,

$$(4.4) \qquad \begin{aligned} &(a)\ u(0) = u_0 + \epsilon_0\{w_1^u \cos \kappa + w_2^u \sin \kappa\} \\ &(b)\ u(1) = u_0 + \epsilon_1 d_1 \end{aligned}$$

and normalization condition,

$$(4.5) \qquad |d_1| = 1$$

Note that $d_1 = (d_{11}, d_{12}, d_{13})$. Perform continuation with respect to $T, \epsilon_1, d_{11}, d_{12}, d_{13}$ using the steering vector algorithm for obtaining an initial orbit as described in [13]. Typically, we use $NMX = 5$ with $NBC = 7, NINT = 0, NTST = 25, NCOL = 5$.

Remark: At Step 1(a), we assume that the solution to Eq. (4.3) remains constant over the interval $T = 0.01$. The tolerances are set to the high value $\epsilon_u, \epsilon_\lambda = 10^{-2}$ in the event that the assumption is not true and the solution does vary substantially

Once the solution reaches Fig. (4.1), AUTO will have computed an accurate enough solution, so that the next step of computation can proceed with much lower tolerances. In fact, in the next step, all we do is to lower the tolerances.

Step 1 (b): At this point AUTO has been able to find an initial orbit, so we decrease the tolerances to $\epsilon_u, \epsilon_\lambda = 10^{-8}$. Perform continuation with respect to $T, \epsilon_1, d_{11}, d_{12}, d_{13}$,

using the same set of boundary conditions as in Step 1(a) until d_1 has approximately the same direction as the eigenvector w_1^s, which defines the direction of the stable manifold near the fixed point. In Fig. (5.2) $T = 4.3, \epsilon_1 = 0.3, d_1 = (7.5 \times 10^{-3}, -2.9 \times 10^{-3}, 0.95)$ and this is a fairly good approximation to the eigenvector $w_1^s = (-5.3 \times 10^{-3}, 5.5 \times 10^{-3}, 0.99)$, which defines the direction of the stable manifold, $W_{loc}^s(u_0)$. At this point we still use pseudo-arclength continuation with $NBC = 7, NINT = 0, NTST = 25, NCOL = 5$. We now attempt to switch from the steering vector to the eigenvector approximation at the boundary $u(1)$.

Remark : It is important to watch the continuation process very carefully in Step 1(b) to see when d_1, is approximately aligned along the eigenvector w_1^s. Fig. (4.3a), shows what happens when $u(1)$ is "too close" to the fixed point for this stage of the continuation ($\epsilon_1 = 0.1$), but $d_1 = (0.04, -0.99, -2.2 \times 10^{-5})$ is a hopeless approximation to $w_1^s = (-5.3 \times 10^{-3}, 5.5 \times 10^{-3}, 0.99)$. We used the 7 boundary conditions of Step 1(b), and attempted to perform continuation with respect to $T, \kappa, d_{11}, d_{12}, d_{13}$ in the hope that the steering vector d_1 would align along the eigenvector w_1^s for some value of κ. Unfortunately, this was not the case. Once $y(t)$ undershoots (falls below the fixed point value on the right boundary $u(1)$) as shown in Fig. (4.3b), it is impossible to compute the homoclinic orbit, no matter how close one is to the fixed point.

Step 2 (a): Switch from the steering vector algorithm to the eigenvector algorithm on the right boundary (stable manifold). i.e. Solve the following equation:

$$\dot{\mathbf{u}} = T\mathbf{f}(\mathbf{u}, \lambda), \quad \mathbf{u} = (x, y, z)$$

(4.6)

with the 6 boundary conditions,

$$(a) \; u(0) = u_0 + \epsilon_0 \{ w_1^u \cos \kappa + w_2^u \sin \kappa \}$$
$$(b) \; u(1) = u_0 + \epsilon_1 d_1$$

(4.7)

9 eigenvalue problem conditions,

$$(a) \; f_u^0 w_1^u = \mu_1^u w_1^u$$
$$(b) \; f_u^0 w_2^u = \mu_2^u w_2^u$$
$$(c) \; f_u^0 d_1 = \mu_1^s d_1$$

(4.8)

3 normalization conditions,

$$(a) \; |w_1^u| = 1$$
$$(b) \; |w_2^u| = 1$$
$$(c) \; |d_1| = 1$$

(4.9)

and the 3 fixed point conditions,

$$(4.10) \qquad\qquad f(u_0, \lambda)$$

We now have a total of 21 boundary conditions. Continuation is carried out with respect to the variables: $T, \epsilon, (\epsilon_1, d_{11}, d_{12}, d_{13}), (\mu_1^u, w_{11}^u, w_{12}^u, w_{13}^u), (\mu_2^u, w_{21}^u, w_{22}^u, w_{23}^u), (u_{01}, u_{02}, u_{03}), \mu_1^s, \kappa$. At this point in the computation, the steering vector has only approximately the same direction as the eigenvector which defines the direction of the stable manifold on the right boundary. Therefore, the tolerances for the state variables and the parameters should be set rather high when switching from the steering vector approximation to the eigenvector approximation. Experimentally we found that we needed $\epsilon_u, \epsilon_\lambda = 1$. Note that Eq. (4.8c) forces a change from the steering vector algorithm to the eigenvector algorithm. After this step of continuation d_1 is aligned along the direction of the eigenvector w_1^s which defines the direction of the stable manifold $W_{loc}^s(u_0)$. We have now reached Fig. (4.4), where $\epsilon_1 = 0.345$ and $d_{11} = -4.87 \times 10^{-3}, d_{12} = 5.06 \times 10^{-3}, d_{13} = 1.0$ are now aligned along the eigenvector w_1^s, but the singular perturbation parameter has changed its value to $\epsilon = 0.0092$. The other parameter values are $d = -0.2, \epsilon = 9.2 \times 10^{-3}, T = 4.3, \epsilon_0 = 10^{-7}, \epsilon_1 = 0.3, \kappa = 5.7 \times 10^{-4}, (\mu_1^s = -2039, d_{11} = -4.9 \times 10^{-3}, d_{12} = 5.1 \times 10^{-3}, d_{13} = 1.0), (\mu_1^u = 4, w_{11}^u = 0.99, w_{12}^u = 0.05, w_{13}^u = -4.9 \times 10^{-4}), (\mu_2^u = 5.99, w_{21}^u = 4.8 \times 10^{-3}, w_{22}^u = 0.99, w_{23}^u = -2.3 \times 10^{-6}), (u_{01} = 1.99, u_{02} = 3.3 \times 10^{-3}, u_{03} = -1.99)$.

Remark: It is also possible to switch from the steering vector approximation to the eigenvector approximation via a *homotopy*.

Step 3 (a): Decrease the tolerances to $\epsilon_u, \epsilon_\lambda = 10^{-1}$, set $NTST = 100, NCOL = 5, DS = -1.0 \times 10^{-4}$ and use *Natural Parameter Continuation* to solve:

$$(4.11) \qquad\qquad u' = Tf(u, \lambda), \quad u = (x, y, z)$$

with the integral phase condition,

$$(4.12) \qquad \int_{-\infty}^{\infty} \left(f(u(t), \lambda) - f(q(t), \lambda^0) \right) \cdot \frac{d}{dt} f(u(t), \lambda) dt = 0$$

the 6 boundary conditions,

$$(4.13) \qquad \begin{aligned} &(a) \ u(0) = u_0 + \epsilon_0 \{ w_1^u \cos \kappa + w_2^u \sin \kappa \} \\ &(b) \ u(1) = u_0 + \epsilon_1 d_1 \end{aligned}$$

9 eigenvalue problem conditions,

$$(4.14) \qquad \begin{aligned} &(a) \ f_u^0 w_1^u = \mu_1^u w_1^u \\ &(b) \ f_u^0 w_2^u = \mu_2^u w_2^u \\ &(c) \ f_u^0 d_1 = \mu_1^s d_1 \end{aligned}$$

3 normalization conditions,

$$(a)\ |w_1^u| = 1$$

(4.15)
$$(b)\ |w_2^u| = 1$$

$$(c)\ |d_1| = 1$$

and the 3 fixed point conditions,

(4.16)
$$f(u_0, \lambda)$$

We now have a total of 21 boundary conditions plus an Integral Phase Condition. Continuation is carried out with respect to the variables: ϵ_1, T, ϵ, (d_{11}, d_{12}, d_{13}), $(\mu_1^u, w_{11}^u, w_{12}^u, w_{13}^u)$, $(\mu_2^u, w_{21}^u, w_{22}^u, w_{23}^u)$, (u_{01}, u_{02}, u_{03}), $\mu_1^s, \kappa, \epsilon_0$. Note that continuation is carried out with ϵ_1 as the primary parameter, which in conjunction with the negative value of DS and *Natural Parameter Continuation*, ensures that the length of the steering vector continuously decreases, pulling the orbit towards the fixed point. Note also that ϵ_0 and κ are allowed to vary so that the correct linear combination of eigenvectors is found on the two dimensional unstable manifold, $W_{loc}^u(\mathbf{u_0})$ to compute an accurate homoclinic orbit.

In Fig. (4.5), the singular perturbation parameter $\epsilon = 9.33 \times 10^{-3}$, $\epsilon_1 = 0.344$. The parameter values are: $d = -0.2, \epsilon = 9.3 \times 10^{-3}, T = 4.3$, $\epsilon_0 = 1.9 \times 10^{-7}, \epsilon_1 = 0.34, \kappa = -5 \times 10^{-6}$, ($\mu_1^s = -2025, d_{11} = -4.9 \times 10^{-3}, d_{12} = 5.1 \times 10^{-3}, d_{13} = 0.99$), ($\mu_1^u = 4, w_{11}^u = 0.99, w_{12}^u = 0.05, w_{13}^u = -4.9 \times 10^{-4}$), ($\mu_2^u = 5.99, w_{21}^u = 4.9 \times 10^{-3}, w_{22}^u = 0.99, w_{23}^u = -2.4 \times 10^{-6}$), ($u_{01} = 1.99, u_{02} = 3.35 \times 10^{-3}, u_{03} = -1.99$). The next step in the computation is to decrease ϵ_1 still more, while simultaneously attempting to increase the accuracy of the computation, which involves decreasing the tolerances $\epsilon_u, \epsilon_\lambda$.

Remark: It was extremely crucial in this step to set $NTST = 100$ to carry out the continuation procedure. From the phase space plot of Fig. (4.5), it is clear that there are several sharp fronts, and this high value of $NTST = 55$ is the only way to accurately compute the solution with these sharp fronts. For example, a value of $NTST = 55$ allowed tolerances of only $\epsilon_u, \epsilon_\lambda = 1$ and this was not sufficiently accurate for continuation.

Step 3(b): The only change from Step (3a) is that we decrease the tolerances and set $\epsilon_u, \epsilon_\lambda = 10^{-8}$. The continuation proceeds as before with Natural Parameter Continuation with respect to the same parameters as in Step (3a). We stop the computation at the point shown in Fig. (4.6), where $\epsilon_0 = 3.7 \times 10^{-9}, \epsilon_1 = 1.0 \times 10^{-7}, \epsilon = 9.3 \times 10^{-3}, T = 5.3$. The parameter values are: $d = -0.2, \epsilon = 9.3 \times 10^{-3}, T = 5.3$, $\epsilon_0 = 3.7 \times 10^{-9}, \epsilon_1 = 1.1 \times 10^{-7}, \kappa = -2.7 \times 10^{-7}$, ($\mu_1^s = -2026, d_{11} = -4.9 \times 10^{-3}, d_{12} = 5.1 \times 10^{-3}, d_{13} = 0.99$), ($\mu_1^u = 4, w_{11}^u = 0.99, w_{12}^u = 0.05, w_{13}^u = -4.9 \times 10^{-4}$), ($\mu_2^u = 5.99, w_{21}^u = 4.9 \times 10^{-3}, w_{22}^u = 0.99, w_{23}^u = -2.4 \times 10^{-6}$), ($u_{01} = 1.99, u_{02} = 3.5 \times 10^{-3}, u_{03} = -1.99$).

Remark: The extremely small values of ϵ_0 and ϵ_1 indicate that the homoclinic orbit has been computed very accurately. In practice, an accuracy of $\epsilon_0, \epsilon_1 = 1.0 \times 10^{-5}$ should suffice.

Step 4: We now attempt to compute a branch of homoclinic orbits with respect to the parameters (d, ϵ) of Eq. (4.1). Deng [12] notes that the homoclinic orbit is

30

twisted for $d = -3.5$ and non-twisted for $d = -0.2$. Consequently, we again use Natural Parameter Continuation to decrease d from -0.2 to -3.5. We use the same set of boundary conditions as in Step (3a) but perform continuation with respect to $d, \epsilon, \epsilon_0, (\epsilon_1, d_{11}, d_{12}, d_{13})$, $(\mu_1^u, w_{11}^u, w_{12}^u, w_{13}^u)$, $(\mu_2^u, w_{21}^u, w_{22}^u, w_{23}^u)$, (u_{01}, u_{02}, u_{03}), μ_1^s, κ. This is now a two parameter continuation problem with respect to the parameters (ϵ, d). The parameter d starts at $d = -0.2$ and continues on until $d = -3.5$ with a significant change in the orbit as shown in Fig. (4.7). The parameter values are: $d = -3.5, \epsilon = 9.3 \times 10^{-3}, \epsilon_0 = 4.7 \times 10^{-9}, \epsilon_1 = 1.1 \times 10^{-7}, \kappa = -1.4 \times 10^{-5}$, $(\mu_1^s = -2024, d_{11} = -5.3 \times 10^{-3}, d_{12} = 5.5 \times 10^{-3}, d_{13} = 1.0$), $(\mu_1^u = 4, w_{11}^u = 0.75, w_{12}^u = 0.66, w_{13}^u = -3.7 \times 10^{-4}$), $(\mu_2^u = 5.9, w_{21}^u = 4.9 \times 10^{-3}, w_{22}^u = 0.99, w_{23}^u = -2.4 \times 10^{-6}$), $(u_{01} = 1.99, u_{02} = 1.99 \times 10^{-3}, u_{03} = -1.99$). The stiffness of the problem is not altered by this variation in the parameter d.

Step 5: Deng [12] notes that a homoclinic orbit exists for $\epsilon = 0.01$. Accordingly, we tried to increase ϵ from $\epsilon = 0.0093$ (in Fig. 4.6) to $\epsilon = 0.01$ using the boundary conditions of Step (2a). We performed continuation with respect to $\epsilon, \epsilon_0, (\epsilon_1, d_{11}, d_{12}, d_{13})$, $(\mu_1^u, w_{11}^u, w_{12}^u, w_{13}^u)$, $(\mu_2^u, w_{21}^u, w_{22}^u, w_{23}^u)$, (u_{01}, u_{02}, u_{03}), μ_1^s, κ using both Pseudo -Arclength Continuation and Natural Parameter Continuation. The continuation process did not converge.

We also attempted to use the boundary conditions of Step (3a) and perform continuation with respect to ϵ, T, $(\epsilon_1, d_{11}, d_{12}, d_{13})$, $(\mu_1^u, w_{11}^u, w_{12}^u, w_{13}^u)$, $(\mu_2^u, w_{21}^u, w_{22}^u, w_{23}^u)$, (u_{01}, u_{02}, u_{03}), μ_1^s, κ, again using both Natural Parameter Continuation and Pseudo-Arclength continuation. Once more, there was no convergence.

A third attempt to perform continuation, which also met with failure was the following: At Step (2a) switch from the steering vector approximation to the eigenvector approximation on the boundary $u(1)$ but hold ϵ constant at $\epsilon = 0.01$ and solve the following problem:

$$u' = Tf(u, \lambda), \quad u = (x, y, z)$$

(4.17)

the 6 boundary conditions,

(4.18)
$$(a) \; u(0) = u_0 + \epsilon_0 \{ w_1^u \cos \kappa + w_2^u \sin \kappa \}$$
$$(b) \; u(1) = u_0 + \epsilon_1 d_1$$

3 eigenvalue problem conditions,

(4.19)
$$f_u^0 d_1 = \mu_1^s d_1$$

and the normalization condition,

(4.20)
$$|d_1| = 1$$

We attempted to perform continuation with respect to ϵ, T, $(\epsilon_1, d_{11}, d_{12}, d_{13})$, μ_1^s, κ but the continuation process did not converge.

We therefore conclude that it is difficult, if not impossible to compute the homoclinic orbit for $\epsilon = 0.01$.

31

4.3 The Methods Which Failed

1. The Homotopy From Two Dimensions

The solution of problems such as the Josephson Junction [11], have been carried out using a homotopy from a known solution to a simpler problem. Since we had already obtained a homoclinic orbit for the simpler two-dimensional problem defined by the system of equations:

$$(4.21) \quad \begin{aligned} \dot{x} &= (2 - z)a(x - 2) + (z + 2)[\alpha(x - x_0) + \beta(y - y_0)] \\ \epsilon\dot{z} &= (4 - z^2)[z + 2 - m(x + 2)] - \epsilon c z \end{aligned}$$

we attempted to find a solution to the system,

$$(4.22) \quad \begin{aligned} \dot{x} &= (2 - z)a(x - 2) + (z + 2)[\alpha(x - x_0) + \beta(y - y_0)] \\ \dot{y} &= \gamma\{(2 - z)[d(b - a)(x - 2)/4 + by] + (z + 2)[-\beta(x - x_0) + \alpha(y - y_0)]\} \\ \epsilon\dot{z} &= (4 - z^2)[z + 2 - m(x + 2)] - \epsilon c z \end{aligned}$$

We initialized $\gamma = 0$, when Eq. (4.22) reduces to Eq. (4.21) and having found a homoclinic orbit for the system of ODEs in Eq. (4.21), we attempted to increase γ from $\gamma = 0$ to $\gamma = 1$, which would give a homoclinic orbit in three dimensions. The advantage of dealing with a two-dimensional problem first, is that the stable and unstable manifolds are one-dimensional, so we do not have to deal with unknown linear combinations of eigenvectors, which is necessary to solve the three dimensional problem. However, this approach did not meet with any success; with hindsight one can see that there is a loop in the three-dimensional orbit shown in Fig. (4.6), which does not exist in the two-dimensional orbit of Fig. (3.5), and this is probably why the homotopy fails.

2. Increasing the Singular Perturbation Parameter ϵ

Apart from the fact, that the linear combination of eigenvectors on the two-dimensional unstable manifold, $W_{loc}^u(u_0)$ is unknown, this problem is compounded by the fact that the system of ODEs is stiff, which makes the problem of computing homoclinic orbits even more difficult. For the two-dimensional system defined by Eq. (4.21), it was found that $|\mu_1^s|$ could be reduced (thus making the system of ODEs less stiff) by increasing the singular perturbation parameter, ϵ. With this "insight", we attempted to increase ϵ using the boundary conditions of Step. (2a) and carrying out continuation with respect to ϵ, T, $(\epsilon_1, d_{11}, d_{12}, d_{13})$, $(\mu_1^u, w_{11}^u, w_{12}^u, w_{13}^u)$, $(\mu_2^u, w_{21}^u, w_{22}^u, w_{23}^u)$, (u_{01}, u_{02}, u_{03}), μ_1^s, κ.

This method failed and the explanation is as follows: It is known theoretically from Deng [12] that a homoclinic orbit exists for $\epsilon = 0.01$, which means that the orbit must intersect the stable manifold $W_{loc}^u(u_0)$ defined by the eigenvector w_1^s at the right boundary $u(1)$. For larger values of ϵ, there is no certainty that the orbit will intersect this one dimensional stable manifold; in fact, in general the orbit will not intersect the one dimensional stable manifold. To guarantee that the orbit intersects the unstable manifold, the manifold would have to be two-dimensional which is not the case for this problem.

32

3. The Initial Value Problem Solver VODE

VODE is an IVP solver designed specifically to tackle systems of stiff ODEs. We intended to compute an initial orbit with VODE for the system in Eq. (4.1), and then perform continuation using AUTO, with respect to the parameters (ϵ, d). VODE was not able to produce the orbits, which were achieved by AUTO in Fig. (4.6). We used the data from Fig. (4.6), namely, $\epsilon = 9.3 \times 10^{-3}, d = -0.2, u_{01} = 1.995, u_{02} = 3.55 \times 10^{-3}, u_{03} - 1.998, w_{11}^u = 0.99, w_{12}^u = 5.21 \times 10^{-4}, w_{13}^u = -4.92 \times 10^{-4}, w_{21}^u = 4.92 \times 10^{-3}, w_{22}^u = 0.99, w_{23}^u = -2.4 \times 10^{-6}, \epsilon_0 = 3.05 \times 10^{-8}, \kappa = -1.89 \times 10^{-6}$. The results of the computation with VODE are shown in Fig. (4.8 a1–c1), and for comparison the results with AUTO are shown in Fig. (4.8 a2–c2). VODE is clearly not able to reproduce the sharp fronts, which can be computed with AUTO and worse still, the computation of $y(t)$ is hopelessly inaccurate.

4.4 Figures.

Fig. 4.1. Initial solution showing $x(t)$ which is constant. $y(t)$ and $z(t)$ are also constant.

Fig. 4.2. $T = 4.3, \epsilon_1 = 0.3, d_1 = \left(7.5 \times 10^{-3}, -2.9 \times 10^{-3}, 0.95\right)$

Fig. 4.3a. A spurious solution plotted in the phase plane

Fig. 4.3b. Graph of $y(t)$ showing undershooting of the y component.

Fig. 4.4. The other parameter values are $d = -0.2, \epsilon = 9.2 \times 10^{-3}, T = 4.3, \epsilon_0 = 10^{-7}, \epsilon_1 = 0.3, \kappa = 5.7 \times 10^{-4}, (\mu_1^s = -2039, d_{11} = -4.9 \times 10^{-3}, d_{12} = 5.1 \times 10^{-3}, d_{13} = 1.0), (\mu_1^u = 4, w_{11}^u = 0.99, w_{12}^u = 0.05, w_{13}^u = -4.9 \times 10^{-4}), (\mu_2^u = 5.99, w_{21}^u = 4.8 \times 10^{-3}, w_{22}^u = 0.99, w_{23}^u = -2.3 \times 10^{-6}), (u_{01} = 1.99, u_{02} = 3.3 \times 10^{-3}, u_{03} = -1.99)$.

Fig. 4.5. The parameter values are: $d = -0.2, \epsilon = 9.3 \times 10^{-3}, T = 4.3, \epsilon_0 = 1.9 \times 10^{-7}, \epsilon_1 = 0.34, \kappa = -5 \times 10^{-6}, (\mu_1^s = -2025, d_{11} = -4.9 \times 10^{-3}, d_{12} = 5.1 \times 10^{-3}, d_{13} = 0.99), (\mu_1^u = 4, w_{11}^u = 0.99, w_{12}^u = 0.05, w_{13}^u = -4.9 \times 10^{-4}), (\mu_2^u = 5.99, w_{21}^u = 4.9 \times 10^{-3}, w_{22}^u = 0.99, w_{23}^u = -2.4 \times 10^{-6}), (u_{01} = 1.99, u_{02} = 3.35 \times 10^{-3}, u_{03} = -1.99)$.

Fig. 4.6. $\epsilon_0 = 3.7 \times 10^{-9}, \epsilon_1 = 1.0 \times 10^{-7}, \epsilon = 9.3 \times 10^{-3}, T = 5.3$. The parameter values are: $d = -0.2, \epsilon = 9.3 \times 10^{-3}, T = 5.3, \epsilon_0 = 3.7 \times 10^{-9}, \epsilon_1 = 1.1 \times 10^{-7}, \kappa = -2.7 \times 10^{-7}$, ($\mu_1^s = -2026, d_{11} = -4.9 \times 10^{-3}, d_{12} = 5.1 \times 10^{-3}, d_{13} = 0.99$), ($\mu_1^u = 4, w_{11}^u = 0.99, w_{12}^u = 0.05, w_{13}^u = -4.9 \times 10^{-4}$), ($\mu_2^u = 5.99, w_{21}^u = 4.9 \times 10^{-3}, w_{22}^u = 0.99, w_{23}^u = -2.4 \times 10^{-6}$), $\left(u_{01} = 1.99, u_{02} = 3.5 \times 10^{-3}, u_{03} = -1.99 \right)$.

Fig. 4.7. The parameter values are: $d = -3.5, \epsilon = 9.3 \times 10^{-3}, \epsilon_0 = 4.7 \times 10^{-9}, \epsilon_1 = 1.1 \times 10^{-7}, \kappa = -1.4 \times 10^{-5}$, ($\mu_1^s = -2024, d_{11} = -5.3 \times 10^{-3}, d_{12} = 5.5 \times 10^{-3}, d_{13} = 1.0$), ($\mu_1^u = 4, w_{11}^u = 0.75, w_{12}^u = 0.66, w_{13}^u = -3.7 \times 10^{-4}$), ($\mu_2^u = 5.9, w_{21}^u = 4.9 \times 10^{-3}, w_{22}^u = 0.99, w_{23}^u = -2.4 \times 10^{-6}$), ($u_{01} = 1.99, u_{02} = 1.99 \times 10^{-3}, u_{03} = -1.99$).

Fig. 4.8 Comparison of results obtained with VODE (a1–c1) and AUTO (a2–c2). The parameter values are $\epsilon = 9.3 \times 10^{-3}, d = -0.2, u_{01} = 1.995, u_{02} = 3.55 \times 10^{-3}, u_{03} - 1.998$, $w_{11}^u = 0.99, w_{12}^u = 5.21 \times 10^{-4}, w_{13}^u = -4.92 \times 10^{-4}, w_{21}^u = 4.92 \times 10^{-3}, w_{22}^u = 0.99, w_{23}^u = -2.4 \times 10^{-6}, \epsilon_0 = 3.05 \times 10^{-8}, \kappa = -1.89 \times 10^{-6}$.
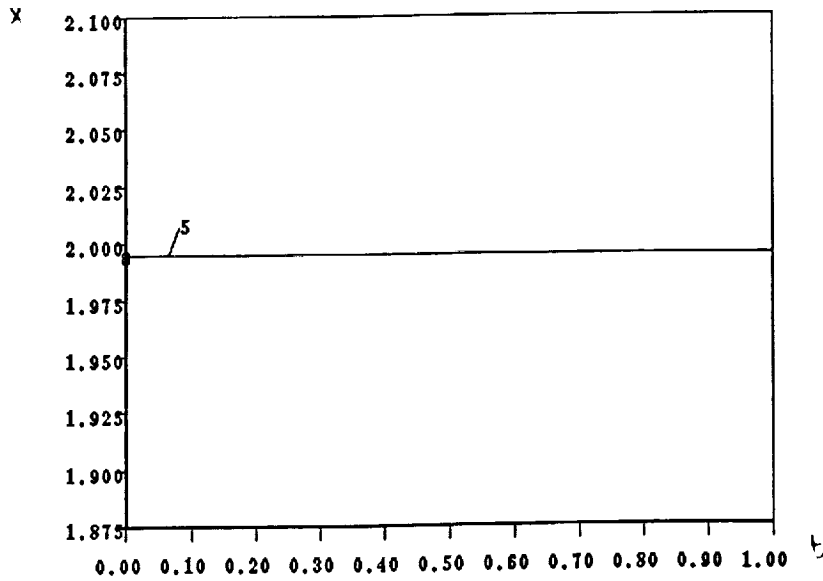
FIGURE 4.1
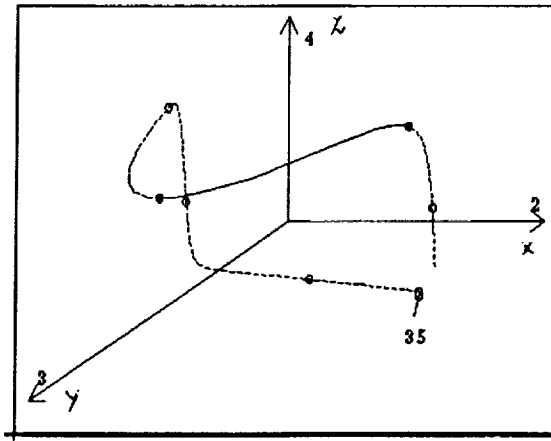
```
THE LABELS ARE :      1    2    3    4    5    6    7    8    9   10
                     11   12   13   14   15   16   17   18   20   21
                     22   23   24   25   26   27   28   29   30   31
                     32   33   34   35   37   38   39   40   42   43
                     44   45   46   47   48   49   50   51   53   54
                     55   56   58   59   60   61   62   63   64   65
                     66   67   68   69   70   71   72   73   74   75
                     76   77   78   79   80   81   82   83   84   85
                     86   87   88   89   90   91

ENTER NEW LABELS :
!5
 DIMENSION ·     4
```
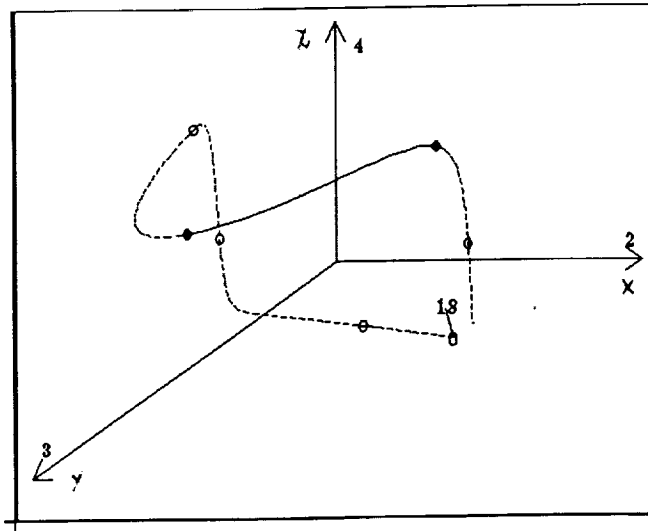
FIGURE 4.2

ENTER COMMAND
d

THE LABELS ARE :   1   2   3   4   5   6   7   8   9   10
                    11   12   13   14   15   16   17   18   20   21
                    22   23   24   25   26   27   28   29   30   31
                    32   33   34   35   37   38   39   40   42   43
                    44   45   46   47   48   49   50   51   53   54
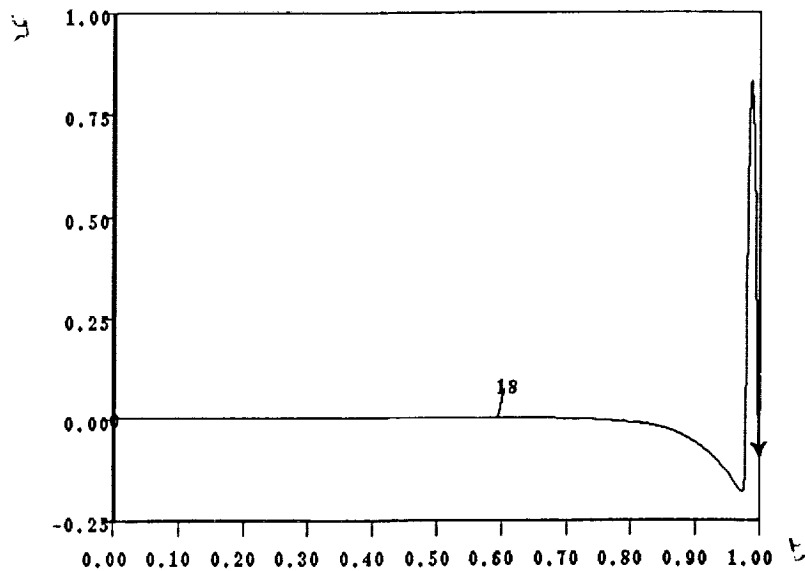
FIGURE 4.3a

FIGURE 4.3b
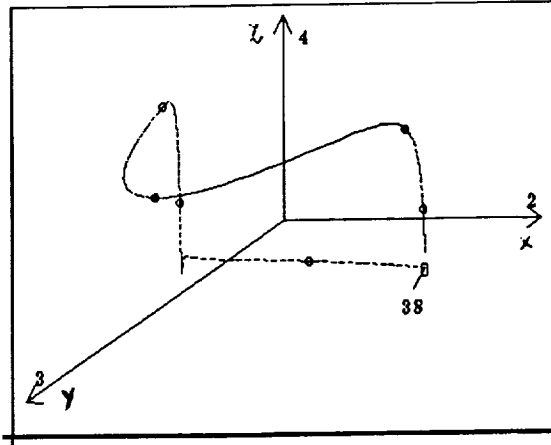
ENTER <3D> COMMAND :
:d
  DIMENSION :   4
  ENTER AXES (DEFAULT   1 2), <D> (DISPLAY), OR <EX> (EXIT)
:d

  THE LABELS ARE :   1   2   3   4   5   6   7   8   9   18
                        11   12   13   14   15   16   17   18   28   21
                        22   23   24   25   26   27   28   29   38   31
                        32   33   34   35   37   38   39   48   42   43
                        44   45   46   47   48   49   58   51   53   54
                        55   56   58   59   68   61   62   63   64   65
                        66   67   68   69   78   71   72   73   74   75
                        76   77   78   79   88   81   82   83   84   85

FIGURE 4.4

```
ENTER <3D> COMMAND :
:d
  DIMENSION :   4
  ENTER AXES  (DEFAULT   1  2),  <D> (DISPLAY), OR <EX> (EXIT)
:d

  THE LABELS ARE :        1     2     3     4     5     6     7     8     9    10
                         11    12    13    14    15    16    17    18    20    21
                         22    23    24    25    26    27    28    29    30    31
                         32    33    34    35    37    38    39    40    42    43
                         44    45    46    47    48    49    50    51    53    54
                         55    56    58    59    60    61    62    63    64    65
                         66    67    68    69    70    71    72    73    74    75
                         76    77    78    79    80    81    82    83    84    85
```

FIGURE 4.5
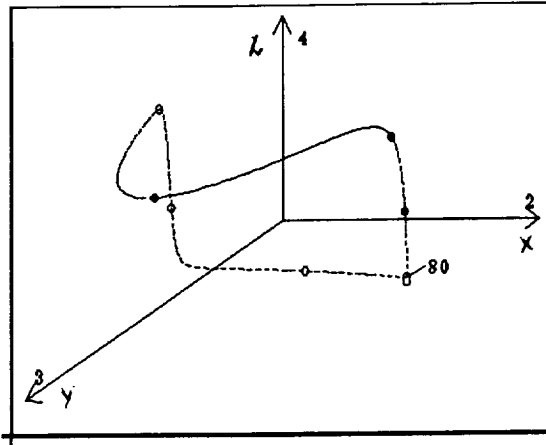
40

```
ENTER <3D> COMMAND :
:d
  DIMENSION :    4
  ENTER AXES  (DEFAULT  1  2),  <D> (DISPLAY), OR <EX> (EXIT)
:d

  THE LABELS ARE :      1    2    3    4    5    6    7    8    9   10
                       11   12   13   14   15   16   17   18   20   21
                       22   23   24   25   26   27   28   29   30   31
                       32   33   34   35   37   38   39   40   42   43
                       44   45   46   47   48   49   50   51   53   54
                       55   56   58   59   60   61   62   63   64   65
                       66   67   68   69   70   71   72   73   74   75
                       76   77   78   79   80   81   82   83   84   85
```

FIGURE 4.6

```
ENTER <3D> COMMAND :
:d
 DIMENSION :    4
 ENTER AXES  (DEFAULT  1 2),  <D> (DISPLAY), OR <EX> (EXIT)
:d

 THE LABELS ARE :    1    2    3    4    5    6    7    8    9   10
                    11   12   13   14   15   16   17   18   20   21
                    22   23   24   25   26   27   28   29   30   31
                    32   33   34   35   37   38   39   40   42   43
                    44   45   46   47   48   49   50   51   53   54
                    55   56   58   59   60   61   62   63   64   65
                    66   67   68   69   70   71   72   73   74   75
                    76   77   78   79   80   81   82   83   84   85
```

FIGURE 4.7

42

THE LABELS ARE :

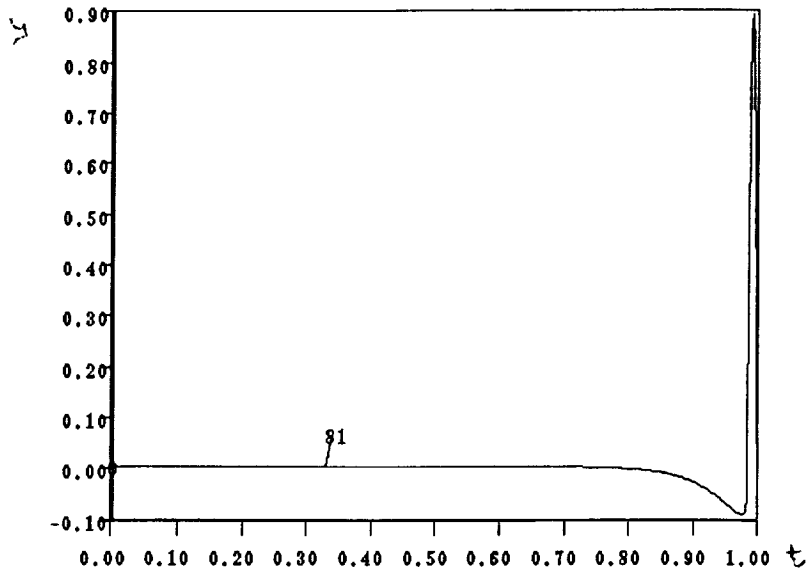| 1	2	3	4	5	6	7	8	9	10
11	12	13	14	15	16	17	18	20	21
22	23	24	25	26	27	28	29	30	31
32	33	34	35	37	38	39	40	42	43
44	45	46	47	48	49	50	51	53	54
55	56	58	59	60	61	62	63	64	65
66	67	68	69	70	71	72	73	74	75

FIGURE 4.8 (a1)

43

Example Epperson (EZA1)

THE LABELS ARE :

1	2	3	4	5	6	7	8	9	10
11	12	13	14	15	16	17	18	20	21
22	23	24	25	26	27	28	29	30	31
32	33	34	35	37	38	39	40	42	43
44	45	46	47	48	49	50	51	53	54
55	56	58	59	60	61	62	63	64	65
66	67	68	69	70	71	72	73	74	75

FIGURE 4.8 (b1)

1	2	3	4	5	6	7	8	9	10
11	12	13	14	15	16	17	18	20	21
22	23	24	25	26	27	28	29	30	31
32	33	34	35	37	38	39	40	42	43
44	45	46	47	48	49	50	51	53	54
55	56	58	59	60	61	62	63	64	65
66	67	68	69	70	71	72	73	74	75

FIGURE 4.8 (c1)

FIGURE 4.8 (a2)

FIGURE 4.8 (b2)

Graph with y-axis labeled z ranging from -2.0 to 2.0, x-axis labeled t ranging from 0.00 to 1.00. A label "81" appears near -1.5 at around 0.35.

```
DIMENSION :    4
ENTER AXES  (DEFAULT   1  2),  <D> (DISPLAY), OR <EX> (EXIT)
d

THE LABELS ARE :     1    2    3    4    5    6    7    8    9   10
                    11   12   13   14   15   16   17   18   20   21
                    22   23   24   25   26   27   28   29   30   31
                    32   33   34   35   37   38   39   40   42   43
```

FIGURE 4.8 (c2)

5. The Fluid Mechanics Problem

5.1 Parameter Assignment in AUTO

For the generic four dimensional problem, the parameter assignment is as follows:

u_0	par(101)-par(104) left fixed point
$\epsilon_{0d}, d_0(4)$	par(106)-par(110) left steering vector
μ_{0i}, w_{0i}	par(111)-par(130) 4 left eigenvalues/vectors
ϵ_{0i}	par(131)-par(135) 4 left eigenvector weights
u_1	par(151)-par(154) right fixed point
$\epsilon_{1d}, d_1(4)$	par(156)-par(160) right steering vector
μ_{1i}, w_{1i}	par(161)-par(180) 4 right eigenvalues/vectors
ϵ_{1i}	par(181)-par(185) 4 right eigenvector weights

ξ_1	par(1)
e_{11}	par(2)
e_{12}	par(3)
ξ_2	par(4)
e_{21}	par(5)
e_{22}	par(6)
s_{34}	par(7) sign for Eqs. (3),(4)

5.2 Formulation of the Problem

We study this system of equations which are discussed in Eq. (2.5) in the paper by Armbruster et al [2]:

$$(a) \quad \dot{x}_1 = x_1 x_2 + y_1 y_2 + x_1(\xi_1 + e_{11}r_1^2 + e_{12}r_2^2)$$
$$(b) \quad \dot{y}_1 = x_1 y_2 - y_1 x_2 + y_1(\xi_1 + e_{11}r_1^2 + e_{12}r_2^2)$$
$$(5.1) \qquad (c) \quad \dot{x}_2 = \pm(x_1^2 - y_1^2) + x_2(\xi_2 + e_{21}r_1^2 + e_{22}r_2^2)$$
$$(d) \quad \dot{y}_2 = \pm 2x_1 y_1 + y_2(\xi_2 + e_{21}r_1^2 + e_{22}r_2^2)$$
$$r_1^2 = x_1^2 + y_1^2 \quad \text{and} \quad r_2^2 = x_2^2 + y_2^2$$

This system of equations corresponds directly to Eq.(28) of Aubry [1]:

$$\dot{v}_2 = c_{4,-2}(v_4 v_2 + w_4 w_2) + v_2(a_2 + d_{22}r_2^2 + d_{24}r_4^2)$$
$$\dot{w}_2 = c_{4,-2}(v_2 w_4 - v_4 w_2) + w_2(a_2 + d_{22}r_2^2 + d_{24}r_4^2)$$
$$(5.2) \qquad \dot{v}_4 = c_{2,2}(v_2^2 - w_2^2) + v_4(a_4 + d_{42}r_2^2 + d_{44}r_4^2)$$
$$\dot{w}_4 = 2c_{2,2}v_2 w_2 + w_4(a_4 + d_{42}r_2^2 + d_{44}r_4^2)$$
$$r_2^2 = v_2^2 + w_2^2 \quad \text{and} \quad r_4^2 = v_4^2 + w_4^2$$

The systems in Eq. (5.1) and Eq. (5.2) are obtained from the Navier-Stokes equations [1]. The fluctuating component of the velocity is expanded as a Fourier series in the spanwise and streamwise directions. A Galerkin projection is applied to convert the system of PDEs into a system of ODEs. The series is then truncated to retain only the first few terms in the Fourier expansion becuase the Galerkin approximation minimizes the error due to truncation. The important parameters in the Armbruster system are ξ_1 and ξ_2, which correspond to the parameters a_2 and a_4 of the Aubry system. a_2 and a_4 are related to the Heisenberg parameters α_1 and α_2 and the Reynolds' number Re_T by the equation:

$$(5.3) \qquad a_k = a_k^1 + (1 + \alpha_1/Re_T)a_k^2$$
$$c_{k',k-k'} = c_{k',k-k'}^1 + \alpha_2 c_{k',k-k'}^2$$

The Heisenberg parameters α_1 and α_2 may be adjusted upward and downward to simulate greater and smaller energy losses to the unresolved modes, corresponding to the presence of a greater or smaller intensity of smaller-scale turbulence in the neighborhood of the wall. This might correspond to the environment just before or just after a bursting event which produces a large burst of small scale turbulence which is then diffused to the outer part of the layer.

We wish to investigate the dynamical behavior of the system defined by Eq. (5.1). The initial value used was directed along w_0^u with $\epsilon_0 = 10^{-7}$ as follows: $u(t) = u_0 + \epsilon_0 w_0$. Continuation was carried out with respect to the period which was initially set at $T = 0.01$ and increased till $T = 130$.

50

The initial values at the left fixed point u_0 were the following:

$$f_u(u_0, \lambda) = \begin{pmatrix} 0.18 & 0 & 0 & 0 \\ 0 & -0.34 & 0 & 0 \\ 0 & 0 & -0.40 & 0 \\ 0 & 0 & 0 & 0 \end{pmatrix}$$

(5.4)

$$w_0^u = (\,1 \quad 0 \quad 0 \quad 0\,)$$

$$\xi_0^u = 0.18$$

$$u_0 = \left(0, 0, \pm(-\mu_2/e_{22})^{1/2}, 0\right)$$

5.3 Computational Results

We use the following notation:

$u_0 = (u_{01}, u_{02}, u_{03}, u_{04})$	Fixed Point near left boundary
$u_1 = (u_{11}, u_{12}, u_{13}, u_{14})$	Fixed Point near right boundary
w_0^u	Eigenvector defining unstable manifold at u_0
μ_0^u	Eigenvalue corresponding to w_0^u
$d_1 = (d_{11}, d_{12}, d_{13}, d_{14})$	Normalized steering vector components connecting u_1 and $u(1)$
ϵ_0	Distance between u_0 and $u(0)$
ϵ_1	Distance between u_1 and $u(1)$

For the system of equations defined by Eq. (5.1) with the negative sign used in Eq. (5.1 c-d), we attempt to generate Fig. (5c) in the paper by Armbruster [2] for which we used the parameter values: $e_{11} = -4, e_{12} = -1, e_{21} = -1, e_{22} = -2, \xi_1 = -0.03, \xi_2 = 0.2$. The unstable manifold $W_{loc}^u(u_0)$ at u_0 is one dimensional and its direction is defined by the eigenvector w_0^u. The stable manifold $W_{loc}^s(u_1)$ at u_1 is two dimensional and since it is difficult to determine the linear combination of eigenvectors which determine its direction we use the steering vector d_1 at this boundary.

Step 1. *Initialize the period T by a "small" number, such as 0.01, and the "distance" ϵ_0 by another "small" number, such as 10^{-7}. Given u_0 and w_0^u, with $|w_0^u| = 1$ initialize the solution by a constant:*

(5.5)
$$u(t) = u_0 + \epsilon_0 w_0^u, \quad 0 < t < 1.$$

and set the tolerances $\epsilon_u = \epsilon_\lambda = 10^{-8}$ and set the number of subintervals and collocation points to $NTST = 25$ and $NCOL = 4$ respectively. Eq. (5.6) and Eq. (5.7) represent a total of 9 boundary conditions. We perform continuation with respect to $(T, \epsilon_1, d_{11}, d_{12}, d_{13}, d_{14})$. We have now reached Fig. (5.1), where $(T = 168, \epsilon_1 = 7.5 \times 10^{-9}, d_{11} = 0.04, d_{12} = 0, d_{13} = 0.99, d_{14} = 0$).

<u>Step 2</u> *We will now attempt to repeat the results of Fig. (5e) in Armbruster [2], where $(\xi_1 = 0.135, \xi_2 = 0.2)$. For these parameter values, modulated travelling waves coexist with the heteroclinic orbit. Moreover it is precisely at these parameter values that a bifurcation occurs from the 2-dimensional heteroclinic orbit shown in Fig. (5.1) (where $(\xi_1 = -0.03, \xi_2 = 0.2)$) to a full 4-dimensional heteroclinic orbit. To reach $(\xi_1 = 0.135, \xi_2 = 0.2)$ we follow a multistep continuation procedure, where the problem is formulated as follows:*

$$(5.6) \qquad u'(t) - Tf(u(t), \lambda) = 0, \quad 0 < t < 1,$$

$$(5.7) \qquad \begin{array}{l} (a) \ f(u_0, \lambda) = 0 \\ (b) \ f(u_1, \lambda) = 0, \end{array}$$

$$(5.8) \qquad \begin{array}{ll} a) & u(0) = u_0 + \epsilon_0 w_0^u, \\ b) & u(1) = u_1 + \epsilon_1 d_1, \qquad d_1 \in \mathbf{R}^n \end{array}$$

$$(5.9) \qquad f_u(u_0, \lambda) w_0^u = \mu_0^u w_0^u, \quad w_0^u \in \mathbf{R}^n, \ \mu_0^u \in \mathbf{R},$$

$$(5.10) \qquad \begin{array}{l} (a) \ |d_1| = 1 \\ (b) \ |w_0^u| = 1, \end{array}$$

$$(5.11) \qquad \int_0^1 \left(f(u(t), \lambda) - f(q(t), \lambda^0) \right) \cdot f_u(u(t), \lambda) f(u(t), \lambda) \, dt = 0.$$

There are 22 boundary conditions plus an Integral Condition. Continuation is performed with respect to the 20 parameters.

Step (2a): Perform continuation with respect to (ξ_1, ξ_2, T), $(u_{01}, u_{02}, u_{03}, u_{04})$, $(u_{11}, u_{12}, u_{13}, u_{14})$, $(d_{11}, d_{12}, d_{13}, d_{14})$, $(\mu_0^u, w_{01}^u, w_{02}^u, w_{03}^u, w_{04}^u)$. The continuation process fails to converge at the terminal values of $(\xi_1 = -3.9 \times 10^{-3}, \xi_2 = 0.198)$, $(T = 124, \epsilon_0 = 10^{-7}, \epsilon_1 = 10^{-6}))$, $(u_{01} = 0, u_{02} = 0, u_{03} = 0.315, u_{04} = 0)$, $(u_{11} = 0, u_{12} = 0, u_{13} = -0.315, u_{14} = 0)$, $(d_{11} = 0.14, d_{12} = -1.4 \times 10^{-8}, d_{13} = 0.98, d_{14} = 0.065)$, $(\mu_0^u = 0.2, w_{01}^u = 1, w_{02}^u = 0, w_{03}^u = 0, w_{04}^u = 0)$.

Step (2b): Using these terminal values, perform continuation with respect to $(\xi_1, \xi_2, \epsilon_0)$, $(u_{01}, u_{02}, u_{03}, u_{04})$, $(u_{11}, u_{12}, u_{13}, u_{14})$, $(d_{11}, d_{12}, d_{13}, d_{14})$, $(\mu_0^u, w_{01}^u, w_{02}^u, w_{03}^u, w_{04}^u)$. The continuation fails to converge at the terminal values $(\xi_1 = 0.1, \xi_2 = 0.21)$, $(T = 124, \epsilon_0 = 8.5 \times 10^{-9}, \epsilon_1 = 10^{-6}))$, $(u_{01} = 0, u_{02} = 0, u_{03} = 0.323, u_{04} = 0)$, $(u_{11} =$

$0, u_{12} = 0, u_{13} = -0.323, u_{14} = 0$), ($d_{11} = 0.79, d_{12} = -6.7 \times 10^{-7}, d_{13} = 0.019, d_{14} = 0.060$), ($\mu_0^u = 0.326, w_{01}^u = 1, w_{02}^u = 0, w_{03}^u = 0, w_{04}^u = 0$).

**Step (2c):** Using these terminal values perform continuation with respect to (ξ_1, ξ_2, ϵ_1), ($u_{01}, u_{02}, u_{03}, u_{04}$), ($u_{11}, u_{12}, u_{13}, u_{14}$), ($d_{11}, d_{12}, d_{13}, d_{14}$), ($\mu_0^u, w_{01}^u, w_{02}^u, w_{03}^u, w_{04}^u$). Continuation proceeds till we reach Fig. (5.2) where ($\xi_1 = 0.138, \xi_2 = 0.21$), ($T = 124, \epsilon_0 = 8.5 \times 10^{-9}, \epsilon_1 = 2.3 \times 10^{-6}$)), ($u_{01} = 0, u_{02} = 0, u_{03} = 0.323, u_{04} = 0$), ($u_{11} = 0, u_{12} = 0, u_{13} = -0.323, u_{14} = 0$), ($d_{11} = 0.96, d_{12} = -8.1 \times 10^{-7}, d_{13} = 4.5 \times 10^{-3}, d_{14} = 0.268$), ($\mu_0^u = 0.326, w_{01}^u = 1, w_{02}^u = 0, w_{03}^u = 0, w_{04}^u = 0$).

Step 3: We will also attempt to reproduce the bifurcation diagram for the branch of heteroclinic orbits, shown in Fig. 3 in Armbruster [2]. Using the same set of boundary conditions as in Step 2, increase the number of subintervals to $NTST = 55$. Using the initial values from Fig. (5.1), perform continuation with respect to (ξ_1, ξ_2, T), ($u_{01}, u_{02}, u_{03}, u_{04}$), ($u_{11}, u_{12}, u_{13}, u_{14}$), ($d_{11}, d_{12}, d_{13}, d_{14}$), ($\mu_0^u, w_{01}^u, w_{02}^u, w_{03}^u, w_{04}^u$). The bifurcation diagram of (ξ_1, ξ_2) is shown in Fig. (5.3), where the initial values are ($\xi_1 = -0.03, \xi_2 = 0.2$) and the final values are ($\xi_1 = -0.036, \xi_2 = 0.09$). The entire bifucation diagram in Fig. (5.3) has a number of bifurcating branches. We have traced out only one branch. This may account for the fact that our results do not match those of Armbruster [2].

5.4 Figures

Fig. 5.1 ($T = 168, \epsilon_1 = 7.5 \times 10^{-9}, d_{11} = 0.04, d_{12} = 0, d_{13} = 0.99, d_{14} = 0$).

Fig. 5.2 ($\xi_1 = 0.138, \xi_2 = 0.21$), ($T = 124, \epsilon_0 = 8.5 \times 10^{-9}, \epsilon_1 = 2.3 \times 10^{-6}$)), ($u_{01} = 0, u_{02} = 0, u_{03} = 0.323, u_{04} = 0$), ($u_{11} = 0, u_{12} = 0, u_{13} = -0.323, u_{14} = 0$), ($d_{11} = 0.96, d_{12} = -8.1 \times 10^{-7}, d_{13} = 4.5 \times 10^{-3}, d_{14} = 0.268$), ($\mu_0^u = 0.326, w_{01}^u = 1, w_{02}^u = 0, w_{03}^u = 0, w_{04}^u = 0$).

Fig. 5.3 The initial values are ($\xi_1 = -0.03, \xi_2 = 0.2$) and the final values are ($\xi_1 = -0.036, \xi_2 = 0.09$).
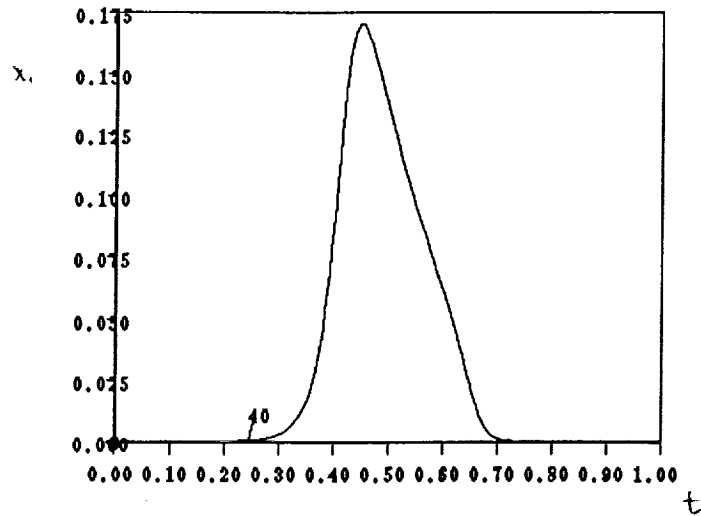
```
THE LABELS ARE :        1    2    3    4    5    6    7    8    9   10
                       11   12   13   14   15   16   17   18   19   20
                       21   22   23   24   25   26   27   28   29   30
                       32   33   34   35   37   38   39   40   41   42
                       43   44   45   46   47   48   49   50   51   52
                       53   54   55
ENTER NEW LABELS :
:6
ERROR - POINT ENTERED NOT IN UNIT 8
 DIMENSION :    3
 ENTER AXES  (DEFAULT   1  2),  <D> (DISPLAY), OR <EX> (EXIT)
```
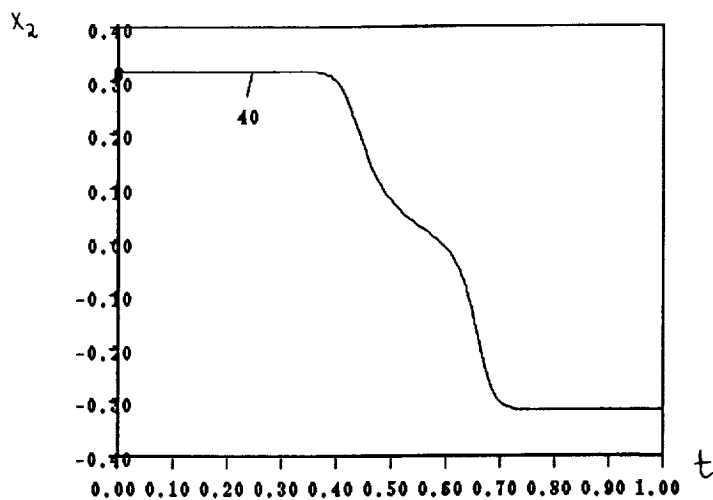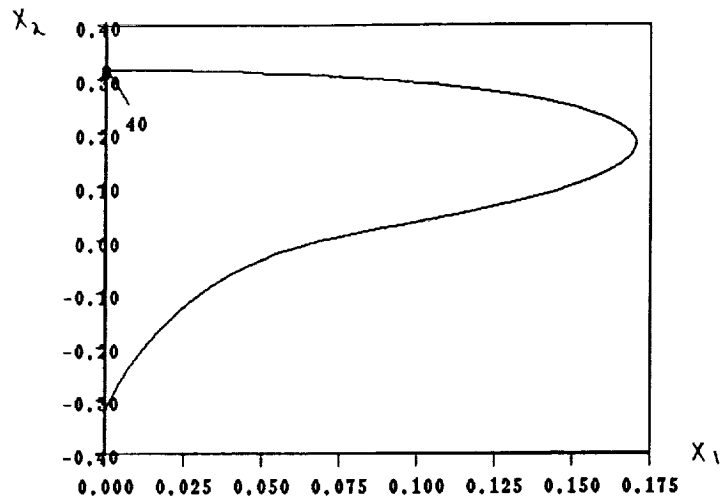
FIGURE 5.1

FIGURE 5.1 (Con't.)

```
ENTER AXES  (DEFAULT   1  2),   <D> (DISPLAY), OR <EX> (EXIT)
I
DIMENSION :    3
ENTER AXES  (DEFAULT   1  2),   <D> (DISPLAY), OR <EX> (EXIT)
. 3
DIMENSION :    3
ENTER AXES  (DEFAULT   1  3),   <D> (DISPLAY), OR <EX> (EXIT)
I
DIMENSION :    3
ENTER AXES  (DEFAULT   1  3),   <D> (DISPLAY), OR <EX> (EXIT)
. 2
DIMENSION :    3
ENTER AXES  (DEFAULT   1  2),   <D> (DISPLAY), OR <EX> (EXIT)
I
```
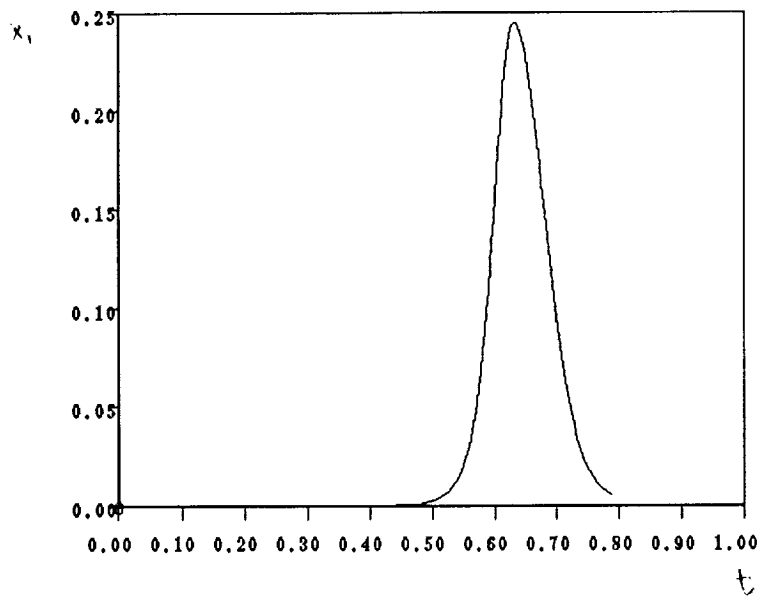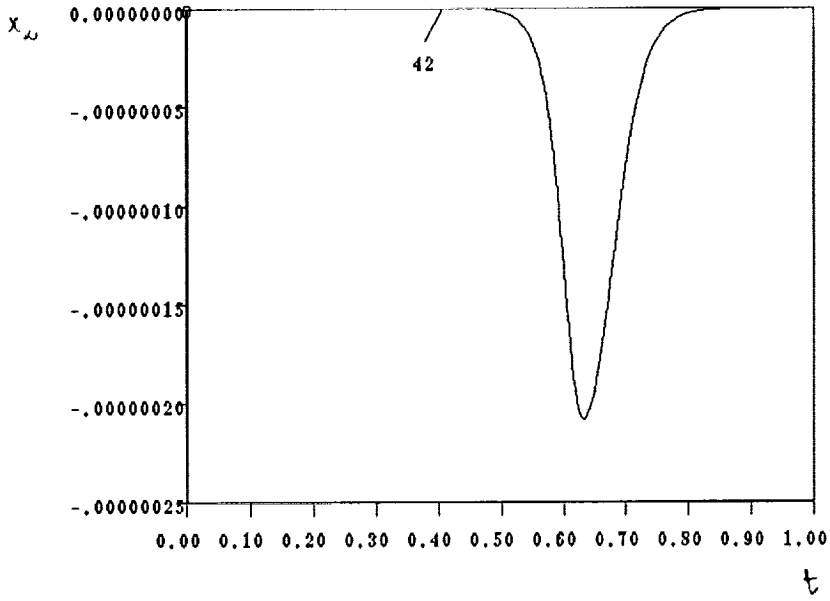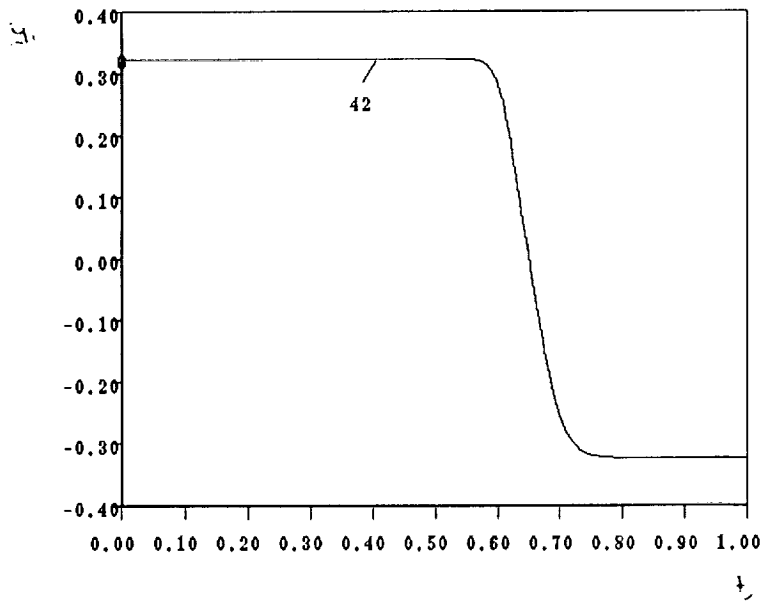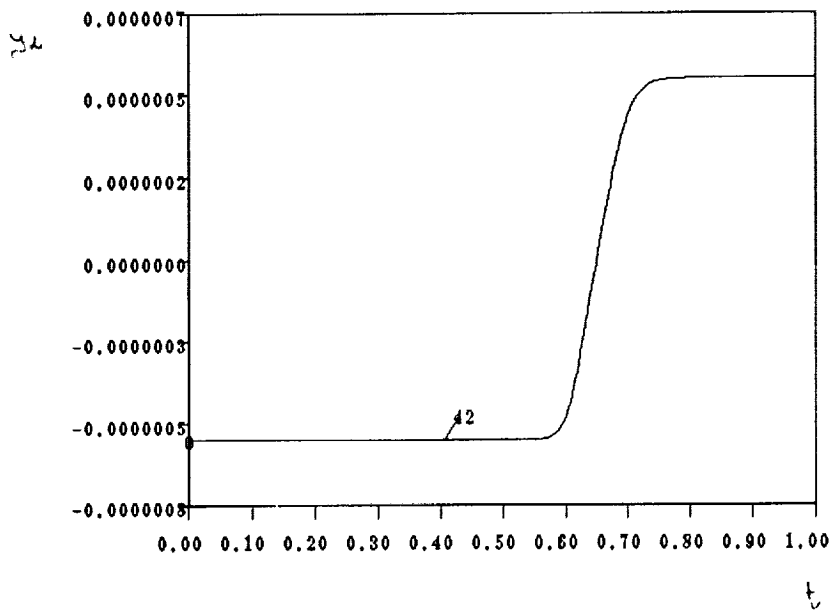
FIGURE 5.1 (Con't.)

FIGURE 5.2

FIGURE 5.2 (Con't.)

FIGURE 5.2 (Con't.)

FIGURE 5.2 (Con't.)
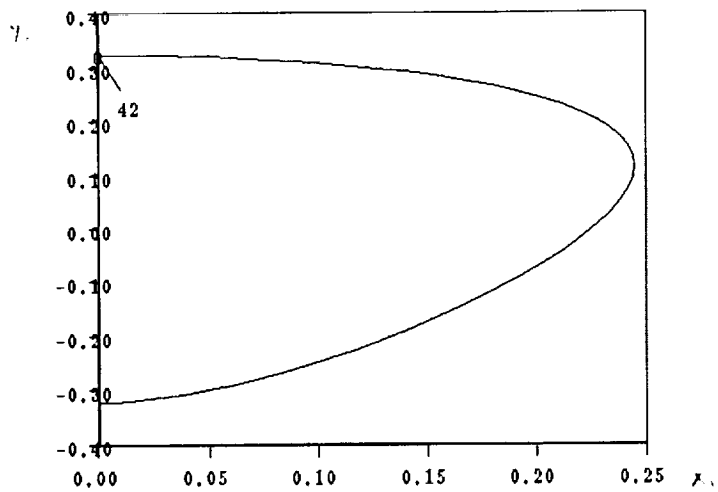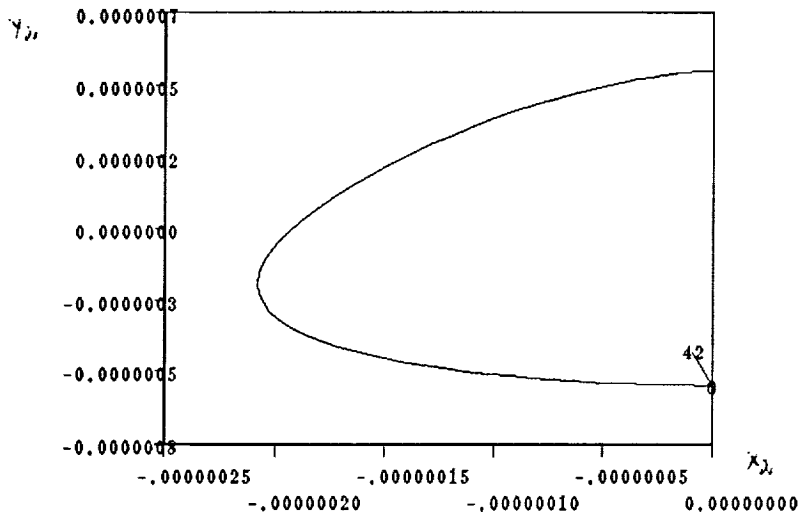
```
ENTER LABELS, OR <A> (ALL)
.2
 DIMENSION :    5
 ENTER AXES  (DEFAULT   1  2),  <D> (DISPLAY), OR <EX> (EXIT)
I
 DIMENSION :    5
 ENTER AXES  (DEFAULT   1  2),  <D> (DISPLAY), OR <EX> (EXIT)
.3
 DIMENSION :    5
 ENTER AXES  (DEFAULT   1  3),  <D> (DISPLAY), OR <EX> (EXIT)
I
 DIMENSION :    5
 ENTER AXES  (DEFAULT   1  3),  <D> (DISPLAY), OR <EX> (EXIT)
```

FIGURE 5.2 (Con't.)

```
ENTER AXES  (DEFAULT   1  2),  <D> (DISPLAY), OR <EX> (EXIT)
. 3
DIMENSION :    5
ENTER AXES  (DEFAULT   1  3),  <D> (DISPLAY), OR <EX> (EXIT)
I
DIMENSION :    5
ENTER AXES  (DEFAULT   1  3),  <D> (DISPLAY), OR <EX> (EXIT)
: 3
DIMENSION :    5
ENTER AXES  (DEFAULT   2  3),  <D> (DISPLAY), OR <EX> (EXIT)
I
DIMENSION :    5
ENTER AXES  (DEFAULT   2  3),  <D> (DISPLAY), OR <EX> (EXIT)
```

FIGURE 5.2 (Con't.)
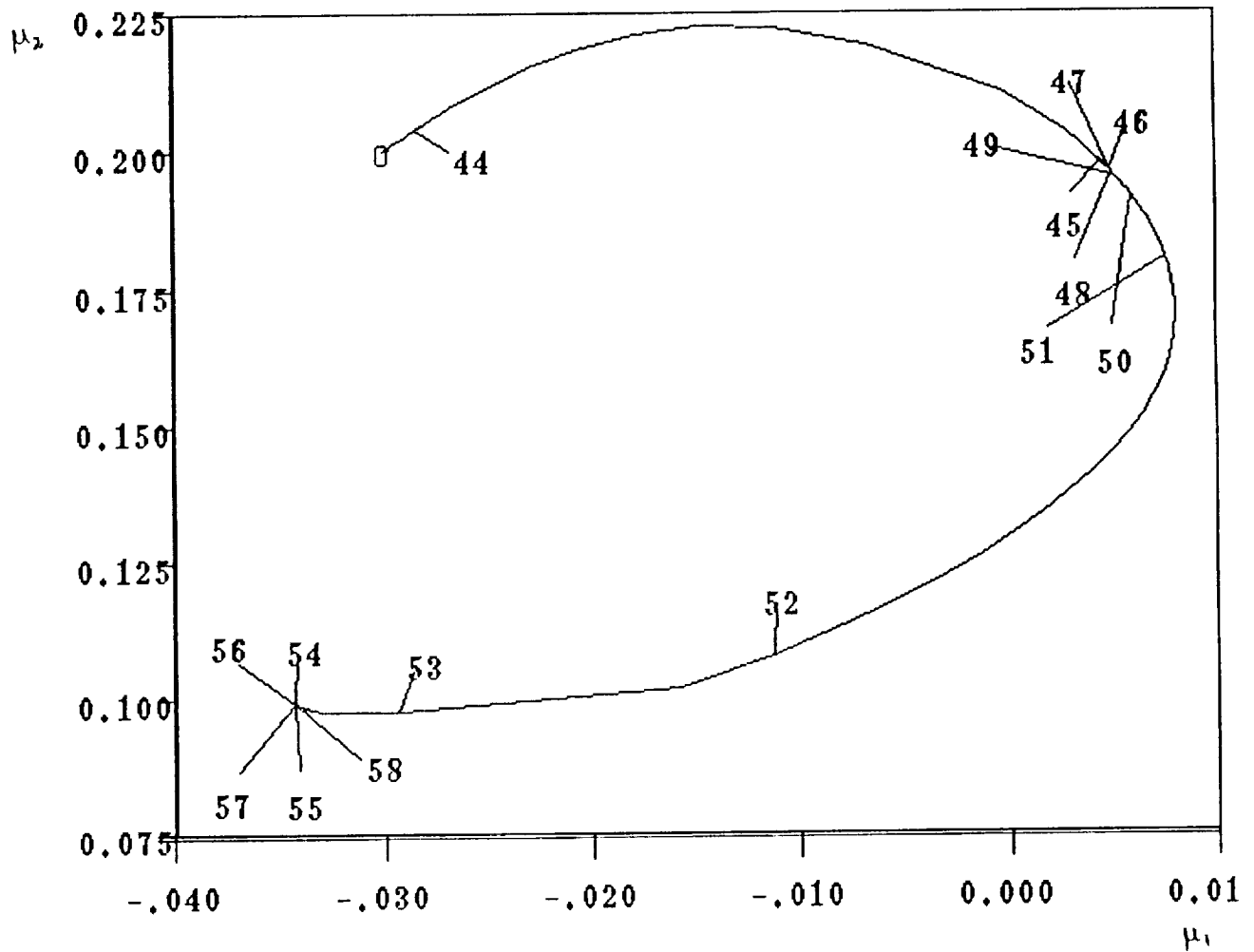
62

FIGURE 5.3

```
math% plaut200.cur
rm: fort.3: No such file or directory
   235   101
   235   101
   235   101
   235   101
   235   101
```

6. Conclusions and Recommendations.

Homoclinic and heteroclinic orbits are orbits of an infinite period connecting two fixed points of an associated system of autonomous ordinary differential equations. Homoclinic orbits have been shown to play a fundamental role in phenomena such as bursting in biology, chaotic vibrations of structures, chaotic oscillations in chemical reactions, etc. Heteroclinic orbits are equally important in the understanding of the global behavior of dynamical systems, turbulence, and also in the study of wave phenomena in nonlinear parabolic partial differential equations.

In earlier papers Doedel and Friedman have developed an accurate, robust, and systematic numerical method and derived error estimates for the computation of branches of homoclinic and heteroclinic orbits. The idea of the method is to reduce a boundary value problem on the real line to a boundary value problem on a finite interval by using a local (linear or higher order) approximation of the stable and unstable manifolds and then study the reduced problem using a continuation software package such as AUTO.

Theoretical analysis of homoclinic and heteroclinic orbits is often conducted in the context of singular perturbation problems. In this paper we have refined and extended ealier algorithms of Doedel and Friedman using 2 model singular perturbation problems and a turbulent fluid boundary layers in the wall region problem. We have thus considerably extended the range of applicability of our algorithms
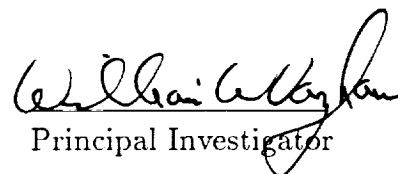
References

[1] N. Aubry et al., "The dynamics of coherent structures in the wall region of a turbulent boundary layer," *J. Fluid Mechanics,* 192 , (1988), 115–173.

[2] D. Armbruster et al., "Heteroclinic Cycles and Modulated Travelling Waves in Systems with O(2) Symmetry," *Physica 29D* (1988), 257–282.

[3] W.-J. Beyn, The numerical computation of connecting orbits in dynamical systems, *IMA J. Numer. Anal.* 9(1990) 379–405.

[4] W.-J. Beyn, Global bifurcations and their numerical computation, in: D. Roose *et al.,* Ed., *Continuation and Bifurcations: Numerical Techniques and Applications* (Kluwer, Dordrecht, Netherlands, 1990, 169–181).

[5] S.N. Chow and X.B. Lin, Bifurcation of a homoclinic orbit with a saddle-node equilibrium, *J. Dif. Int. Eqas.* 3 (1990) 435–466.

[6] J. Descloux and J. Rappaz, Approximation of solution branches of nonlinear equations, *R.A.I.R.O.* 16 (1982) 319–349.

[7] E.J. Doedel and M.J. Friedman, Numerical computation of heteroclinic orbits, J. Comput. and Appl. Math. 26 (1989) 159–170.

[8] E.J. Doedel and M.J. Friedman, Numerical computation and continuation of invariant manifolds connecting fixed points with application to computation of combustion fronts, in: T. J. Chung, G. R. Karr, Eds., *Proc. 7th Int. Conf. on Finite Element Methods in flow problems* (UAH Press, Huntsville, AL, 1989, 277-282).

[9] E.J. Doedel and J.P. Kernevéz, AUTO: *Software for continuation and bifurcation problems in ordinary differential equations,* Applied Mathematics Report, California Institute of technology, 1986, 226 pages.

[10] M.J. Friedman and E.J. Doedel, Numerical computation and continuation of invariant manifolds connecting fixed points, *SIAM J. Numer. Anal.* 28, No. 3 (1991), 789–808.

[11] M.J. Friedman and E.J. Doedel, Computational methods for global analysis of homoclinic and heteroclinic orbits: a case study, to appear in J. of Dynamics and Dif. Equations.

[12] B. Deng, " Constructing Homoclinic Orbits and Chaos", preprint (1991)

[13] A.C. Monteiro, "Algorithms for Computing Heteroclinic Orbits", M.S. thesis, Department of Mathematical Sciences, University of Alabama in Huntsville, 1992.

[14] J. Guckenheimer and S. Kim, KAOS: Dynamical System Toolkit with Interactive Graphic Interface, Mathematics Department, Cornell University, January 1990.

[15] P. C. Brown, G. D. Byrne, and A. C. Hindmarsh, "VODE: A variable Coefficient ODE Solver, " SIAM J. Sci. Stat. Comput., 10 (1989), 1038–1051.

[16] M.J. Friedman, Numerical analysis and accurate computation of heteroclinic orbits in the case of center manifolds, to appear in J. of Dynamics and Dif. Equations.

This technical report was prepared by the Research Institute of The University of Alabama in Huntsville. This report is to serve as documentation of technical work performed under contract number NAS8-36955, Delivery Order 65. Dr. William W. Vaughan was principal investigator. Technical work was produced by Dr. Mark Friedman and Mr. Anand Monteiro. Dr. George Fichtl of the Space Laboratory provided technical coordination.

The views, opinions and/or findings contained in this report are those of the author(s) and should not be construed as an official NASA position, policy or decision unless so designated by other official documentation.

Prepared for:
NASA (sp out)
Marshall Space Flight Center

I have reviewed this report, dated _10 September 1992_ and the report contains no classified information.

William Vaughan

Principal Investigator

66

REPORT DOCUMENTATION PAGE	Form Approved OMB No 0704-0188

1. AGENCY USE ONLY (Leave blank)	2. REPORT DATE March 1993	3. REPORT TYPE AND DATES COVERED Contractor Report (Final Report)

4. TITLE AND SUBTITLE

Accurate Computation and Continuation of Homoclinic and Heteroclinic Orbits for Singular Perturbation Problems

6. AUTHOR(S)

M. J. Friedman and A. C. Monteiro

5. FUNDING NUMBERS

NAS8-36955, Delivery Order 65

Technical Report #5-32341

7. PERFORMING ORGANIZATION NAME(S) AND ADDRESS(ES)

Mathematical Sciences Department
The University of Alabama in Huntsville
Huntsville, AL 35899

8. PERFORMING ORGANIZATION REPORT NUMBER

M-717

9. SPONSORING / MONITORING AGENCY NAME(S) AND ADDRESS(ES)

National Aeronautics and Space Administration
George C. Marshall Space Flight Center
Marshall Space Flight Center, AL 35812

10. SPONSORING / MONITORING AGENCY REPORT NUMBER

NASA CR-4503

11. SUPPLEMENTARY NOTES

12a. DISTRIBUTION / AVAILABILITY STATEMENT

Unclassified—Unlimited

Subject Category: **64**

12b. DISTRIBUTION CODE

13. ABSTRACT (Maximum 200 words)

In earlier papers (see [11] and references therein) Doedel and the authors have developed a numerical method and derived error estimates for the computation of branches of heteroclinic orbits for a system of autonomous ordinary differential equations in R^n. The idea of the method is to reduce a boundary value problem on the real line to a boundary value problem on a finite interval by using a local (linear or higher order) approximation of the stable and unstable manifolds. A practical limitation for the computation of homoclinic and heteroclinic orbits has been the difficulty in obtaining starting orbits. Typically these were obtained from a closed form solution or via a homotopy from a known solution. Here we consider extensions of our algorithm which allow us to obtain starting orbits on the continuation branch in a more systematic way as well as make the continuation algorithm more flexible. In applications we use the continuation software package AUTO in combination with some initial value software. The examples considered include computation of homoclinic orbits in a singular perturbation problem and in a turbulent fluid boundary layer in the wall region problem.

14. SUBJECT TERMS

Heteroclinic Orbits, Computation and Continuation, Singular Perturbation

15. NUMBER OF PAGES 76

16. PRICE CODE A05

17. SECURITY CLASSIFICATION OF REPORT	18. SECURITY CLASSIFICATION OF THIS PAGE	19. SECURITY CLASSIFICATION OF ABSTRACT	20. LIMITATION OF ABSTRACT
Unclassified	Unclassified	Unclassified	Unlimited